Buss, H. L., Lüttge, A., & Brantley, S. L. (2007). Etch pit and leached layer formation on iron-silicate surfaces during siderophore-promoted dissolution. Chemical Geology, 240(3-4), 326-342. 10.1016/j.chemgeo.2007.03.003

Elsevier Editorial System(tm) for Chemical Geology

Manuscript Draft

Manuscript Number: CHEMGE3435R1

Title: Etch pit formation on iron silicate surfaces during siderophore-promoted dissolution

Article Type: Research Article

Section/Category:

Keywords: siderophores; etch pits; hornblende; desferrioxamine; EPS; extracellular polysaccharides; biofilms

Corresponding Author: Dr. Heather L. Buss, PhD

Corresponding Author's Institution: U.S. Geological Survey

First Author: Heather L. Buss, PhD

Order of Authors: Heather L. Buss, PhD; Susan L Brantley; Andreas Luttge

Manuscript Region of Origin:

Abstract: Understanding the effects of microbiota on mineral alteration requires the ability to recognize evidence of bacteria-promoted dissolution on mineral surfaces. Although siderophores are known to promote mineral dissolution, their effects on mineral surfaces are not well known. We have utilized atomic force microscopy (AFM), X-ray photoelectron spectroscopy (XPS), and Mirau vertical scanning interferometry (VSI) to investigate surfaces after incubation with the siderophore desferrioxamine-B mesylate (DFAM) and under colonies of bacteria. Iron-silicate glass planchets chemically similar to hornblende were incubated in buffered growth medium with siderophore-producing bacteria (Bacillus sp.) for 46 days with parallel abiotic experiments conducted with and without 240 μM DFAM, with and without 0.01 g/l of microbially produced extracellular polysaccharides (EPS, alginate or xanthan gum). Some glass planchets were protected by dialysis tubing from direct contact with the EPS. Weekly sampling and analysis of all filtered sample solutions showed negligible Fe and Al release in the control experiments and significant release of Fe and Al in the presence of DFAM, with negligible changes in pH. Concentration of Fe in the filtered solutions after incubation with bacteria was below detection, consistent with uptake of Fe by cells. Release of Fe, Al, and Si in control, xanthan-only, and alginate-only experiments was negligible. Release of these elements was enhanced in all experiments containing DFAM, and greatest in alginate + DFAM experiments.
AFM and VSI analyses reveal widespread, small etch pits and greater root mean squared roughness on siderophore-exposed surfaces and fewer, localized, larger etch pits on bacteria-exposed surfaces. This is the first documented case of etch pit development during siderophore-promoted dissolution. Roughness was not affected by growth medium or alginate or xanthan gum alone. The roughness trends among samples correlate with trends in Fe depletion documented by XPS. Enhanced dissolution and roughness cannot be attributed to direct contact with EPS

because no significant chemical or physical differences were observed between surfaces directly exposed to EPS and those protected by dialysis tubing. Acetate released from the EPS may have enhanced the siderophore-promoted dissolution. Siderophores produced by Bacillus sp. may be responsible for some of the 'biopits.' The difference in size and distribution of the biopits may be related to colonization.

Revision for Chemical Geology

Etch pit formation on iron silicate surfaces during siderophore-promoted dissolution

Heather L. Buss[a*1], Andreas Lüttge[b], and Susan L. Brantley[c]

[a]Department of Geosciences, the Pennsylvania State University, University Park, Pennsylvania 18802 USA, hlbuss@usgs.gov

[b]Department of Earth Science MS-126, Rice University, 6100 Main Street, Houston, Texas 77005 USA, aluttge@rice.edu

[c]Earth and Environmental Systems Institute, the Pennsylvania State University, University Park, Pennsylvania 16802 USA, brantley@eesi.psu.edu

February 18, 2007

*Corresponding author, email: hlbuss@usgs.gov, tel: 650-329-4420, fax: 650-329-4538

[1]Present address: U.S. Geological Survey, Water Resources Discipline, 345 Middlefield Rd., MS 420, Menlo Park, California 94025 USA

Abstract

Understanding the effects of microbiota on mineral alteration requires the ability to recognize evidence of bacteria-promoted dissolution on mineral surfaces. Although siderophores are known to promote mineral dissolution, their effects on mineral surfaces are not well known. We have utilized atomic force microscopy (AFM), X-ray photoelectron spectroscopy (XPS), and Mirau vertical scanning interferometry (VSI) to investigate surfaces after incubation with the siderophore desferrioxamine-B mesylate (DFAM) and under colonies of bacteria. Iron-silicate glass planchets chemically similar to hornblende were incubated in buffered growth medium with siderophore-producing bacteria (*Bacillus* sp.) for 46 days with parallel abiotic experiments conducted with and without 240 µM DFAM, with and without 0.01 g l^{-1} of microbially produced extracellular polysaccharides (EPS, alginate or xanthan gum). Some glass planchets were protected by dialysis tubing from direct contact with the EPS. Weekly sampling and analysis of all filtered sample solutions showed negligible Fe and Al release in the control experiments and significant release of Fe and Al in the presence of DFAM, with negligible changes in pH. Concentration of Fe in the filtered solutions after incubation with bacteria was below detection, consistent with uptake of Fe by cells. Release of Fe, Al, and Si in control, xanthan-only, and alginate-only experiments was negligible. Release of these elements was enhanced in all experiments containing DFAM, and greatest in alginate + DFAM experiments.

AFM and VSI analyses reveal widespread, small etch pits and greater root mean squared roughness on siderophore-exposed surfaces and fewer, localized, larger etch pits on bacteria-exposed surfaces. This is the first documented case of etch pit development during siderophore-promoted dissolution. Roughness was not affected by the growth medium, alginate, or xanthan gum alone. The roughness trends among samples correlate with trends in Fe depletion

documented by XPS. Enhanced dissolution and roughness cannot be attributed to direct contact with EPS because no significant chemical or physical differences were observed between surfaces directly exposed to EPS and those protected by dialysis tubing. Acetate released from the EPS may have enhanced the siderophore-promoted dissolution. Siderophores produced by *Bacillus* sp. may be responsible for some of the 'biopits.' The difference in size and distribution of the biopits may be related to colonization.

Keywords: siderophores, etch pits, hornblende, desferrioxamine, biofilms

1. Introduction

1.1 Surface Colonization

Microbial colonization of mineral surfaces is rapid and extensive in aqueous and soil environments because organic macromolecules adsorb to surfaces and form a layer that encourages attachment of microorganisms (Baier, 1980; Brisou, 1995; Characklis, 1989; Little et al., 1997). As a result, free microorganisms represent only 0.1 to 1.0 % of total microorganisms in an aquatic ecosystem, with the remainder of the microorganisms attached to surfaces (Brisou, 1995; Madigan et al., 2000).

To colonize a surface, microorganisms form large aggregates of cells, proteins, lectins, and polysaccharides, collectively termed "biofilms" (e.g., Brisou, 1995; Little et al., 1997; e.g., Wilderer and Characklis, 1989). A number of researchers have documented the attachment of microorganisms to mineral surfaces via the formation of a biofilm (e.g., Barker et al., 1998; e.g., Thorseth et al., 1995). The nutrient content of mineral surfaces drives the attachment (Bennett et al., 1996a; Brisou, 1995; Madigan et al., 2000). In fact, in environments depleted in one or more

nutrients, microorganisms preferentially colonize mineral surfaces containing essential macro- or micronutrients (Bennett et al., 1996a; Grantham and Dove, 1996; Kalinowski et al., 2000; Rogers et al., 1998; Sawyer and Hermanowicz, 1998).

The effects of colonization on mineral surfaces remain, for the most part, un-quantified. Effects such as the formation of etch pits by microorganisms on mineral surfaces are of interest as potential biosignatures. Several researchers have documented etch pits on colonized mineral surfaces using scanning electron, transmission electron, vertical scanning interferometry or atomic force microscopies (SEM, TEM, VSI, AFM, respectively). Barker et al. (1998) and Rogers et al. (1998) saw etch pits on feldspars near attached microbial colonies. Fisk et al. (1998) observed remnants of cells within etched channels on basaltic glass collected from the sea floor and found the etchings to be consistent with microbial weathering. Similarly, Furnes et al. (2004) found tubular and segmented etchings that were likely microbial in origin on formerly glassy rims of Archean pillow basalts. Irregular etchings on hematite particles (Maurice et al., 1996) and muscovite surfaces (Maurice et al., 2001) were observed after incubation with bacteria in laboratory and field experiments, respectively. Others have documented etch pits on surfaces from which colonies have been removed (Bennett et al., 1996a; Thorseth et al., 1995). Whether the etch pits were formed by way of direct cellular attachment or chemical interactions with one or more microbial exudates is unknown. Conversely, Lüttge and Conrad (2004) found bacteria to inhibit etch pit formation on calcite surfaces.

Microorganisms produce and secrete a variety of substances that may influence mineral dissolution by lowering pH, by complexing with surface or solution ions, or by catalyzing redox reactions. Some of these substances include enzymes, alcohols, low molecular weight organic acids (LMWOA), high molecular weight extracellular polymeric substances (EPS), and highly

Fe(III)-specific ligands called siderophores. Some high affinity ligands may also be released to extract other metals (e.g., Liermann et al., 2005).

The EPS that bacteria secrete are primarily composed of glycocalyx, which are primarily polysaccharides and serve to anchor and give structure to the biofilm and to concentrate and store enzymes, ions, other bioessential molecules, and heavy metals (Brisou, 1995; Madigan et al., 2000; Morel and Palenik, 1989; Roane and Kellogg, 1996; Templeton et al., 2003).

1.2 Siderophores

Most microorganisms need ~μM concentrations of Fe to thrive (Neilands, 1995). Fe(III)-oxides (including oxides, oxyhydroxides, and hydrated oxides), specifically goethite (α-FeOOH), are the dominant forms of Fe in most aerobic soils (Hersman, 2000). Fe in these secondary minerals ultimately derives from the common rock-forming Fe-silicates: olivines, pyroxenes, amphiboles (notably hornblende), and biotite (Allen and Hajek, 1989; Huang, 1989). In soils containing these primary Fe minerals, the actions of microorganisms may affect silicate weathering rates (e.g., Bennett et al., 1996b; Buss et al., 2005; Liermann et al., 2000b) with implications for the global regulation of CO_2 over geologic timescales (e.g., Berner, 1995). However, the low solubility products of most Fe-minerals and especially Fe(III)-oxides, limit the aqueous Fe concentration at equilibrium and near-neutral pH to as low as 10^{-17} M in inorganic solutions (Schwartzman and Volk, 1991). Many microorganisms have evolved the ability to produce siderophores in order to overcome the ~10 orders of magnitude difference between available Fe and Fe needed for metabolism (Hersman, 2000).

109 Typical aqueous siderophore concentrations in nature are estimated to range from
110 approximately equal to as much as three orders of magnitude less than concentrations of
111 other chelators in soils, such as LMWOA (Hersman et al., 1995; Hersman, 2000;
112 Kalinowski et al., 2000). LMWOA can increase weathering via proton- or ligand-
113 promoted dissolution. However, siderophores have greater affinity for Fe than LMWOA
114 and previous studies have shown that siderophores are more effective than LMWOA for
115 inducing release of Fe(III) from minerals at near neutral pH (Brantley et al., 2001;
116 Holmen and Casey, 1996; Kalinowski et al., 2000).

117 Here we investigate the effects on Fe-silicate surfaces of siderophores, EPS, and
118 microorganisms that only use Fe as a micronutrient (i.e., that do not respire Fe). We
119 performed batch dissolution experiments in which flasks containing a polished Fe-silicate
120 substrate and an Fe-free, buffered, pH-neutral growth medium were each supplemented
121 with desferrioxamine-B mesylate (DFAM, the salt of a commercially available
122 siderophore) or a strain of *Bacillus* sp., an obligately aerobic soil bacterium that produces
123 an acidic glycocalyx (Brantley et al., 2001) and a catecholate siderophore (Kalinowski et
124 al., 2000). To more specifically investigate the influence of EPS on siderophore-
125 promoted dissolution, we also incubated hornblende glass planchets in batch experiments
126 with alginate or xanthan gum (Sigma), two commercially available extracellular
127 polysaccharides, with and without DFAM.

128 Surfaces were analyzed with AFM, Mirau vertical scanning interferometry (VSI), and XPS
129 to document changes in microtopography and chemistry of the surfaces. Solution analyses were
130 performed to document glucose consumption, pH changes, and Fe, Al, and Si release.

2. Materials and Methods

2.1 Experimental Setup

In order to isolate biogenic features from mineralogical features (e.g., heterogeneities among crystals, preferential dissolution of inclusions or along crystal grain boundaries), glass planchets were synthesized with a composition similar to the Fe-silicate mineral hornblende (Liermann et al., 2000a) and polished to provide a smooth, chemically analogous substrate. The composition of this "hornblende glass" (in wt%: 48.2% SiO_2, 14.5% Al_2O_3, 11.0% Fe_2O_3, 8.33% CaO, 10.9% MgO, 2.31% Na_2O, 0.51% K_2O, where Fe_2O_3 includes Fe(II) and Fe(III)) was determined using the lithium metaborate fusion technique (Medlin et al., 1969; Suhr and Ingamells, 1966) and inductively coupled plasma atomic emission spectrometry (ICP-AES). The glass was cut into planchets approximately 1 x 1 x 0.5 cm with a diamond blade and polished with diamond slurries to 0.25 μm. Polished samples were ultrasonicated in acetone for 10 minutes, air-dried, and stored in a dessicator.

The soil bacterium selected for this study was previously identified as an Arthrobacter but was subsequently found to be a *Bacillus* sp. (Buss et al., 2003). This bacterium was isolated from a hornblende-containing soil from Gore Mountain, New York, and has been shown to grow vigorously and produce siderophores in Fe-deficient growth medium in the presence of hornblende or hornblende glass (Brantley et al., 2001; Kalinowski et al., 2000; Liermann et al., 2000a). Two polished hornblende glass planchets were placed in each 500-ml glass culture flask and sterilized by autoclaving at 250°C for 20 minutes. After cooling, 150 ml of sterilized, modified iron-free MM9 medium (Liermann et al., 2000a; Schwyn and Neilands, 1987) was added aseptically. The medium composition was: 6.0 g l^{-1} Na_2HPO_4, 0.3 g l^{-1} KH_2PO_4, 0.5 g l^{-1}

NaCl, 1.0 g l^{-1} NH_4Cl, and 6.06 g l^{-1} (50 mM) TRIS buffer, prepared from ultrapure chemicals and deionized water and buffered at pH 7.4. The medium was supplemented with 2% (v/v) Chelex-100-treated 10% (w/v) casamino acids (Bio-Rad Laboratories, Difraco Laboratories, respectively), 0.2% (v/v) 1M $MgSO_4$, 1% (v/v) filter-sterilized 20% (w/v) glucose, and 0.01% (v/v) 1M $CaCl_2$, each prepared and sterilized separately. Some experiments were supplemented with filter-sterilized 240 µM DFAM, or sterilized 0.1 g ml^{-1} alginate or xanthan gum. Alginates are polysaccharides produced by several species of bacteria and algae. These polymers contain monomers of D-mannosyluronic and L-gulosyluronic acids (Budavari, 1996) or β-D-mannuronic and α-L-guluronic acids (Larsen and Haug, 1971). Xanthan gum is produced by *Xanthomonas campestris* and is composed of monomers of D-glucose, D-mannose, and D-glucuronic acid (Sloneker and Jeanes, 1962). The mannuronic acid and guluronic acid monomers of alginate have pKa's of 3.38 and 3.65, respectively and the glucose, mannose, and glucuronic acid monomers of xanthan gum have pKa's of 12.28, 12.08, and ~2.9, respectively (Rohrer and Olechno, 1992; Wang et al., 1991). The pKa's of these polymers' acid groups are below the experimental pH of 7.4 indicating that they remain deprotonated during the experiments. Although the protonation constants for DFAM are relatively high (pKa's of 8.50, 9.24, and 9.69), protonation occurs at non-chelating amino groups and thus does not interfere with Fe(III) chelation at pH values below the pKa's (Winkelmann, 1991).

Duplicate flasks for each of six conditions were set up. Abiotic conditions included 1) controls (medium + planchets), 2) DFAM-only (medium + planchets + DFAM), 3) xanthan-only (medium + planchets + xanthan gum), 4) alginate-only (medium + planchets + alginate), 4) xanthan + DFAM (medium + planchets + xanthan gum + DFAM), and 5) alginate + DFAM (medium + planchets + alginate + DFAM). To determine whether direct attachment to mineral

surfaces is required for EPS to affect dissolution, in the flasks with EPS (alginate or xanthan gum) one of the two glass planchets was enclosed in 12 – 14,000 Dalton dialysis tubing. The molecular weights of alginate and xanthan gum are about 240,000 and > 10^6 Daltons, respectively (Budavari, 1996). Thus, the dialysis tubing prevented the polymers from contacting the surfaces while permitting free flow of siderophores and other small molecules and ions. A sixth set of 2 flasks contained live bacteria (medium + planchets + 2.0 ml of an inoculum of stationary stage cultures of *Bacillus* sp.). Inocula contained 2.5 x 10^7 cells ml^{-1}, as counted on streak plates. All experiments were incubated at room temperature for 46 days on a shaker table continuously agitated at 120 rpm.

To monitor chemical changes over time and to replenish nutrients to sustain microbial growth, solutions were aseptically sampled from each flask and replaced with equivalent amounts of fresh medium ± DFAM ± EPS approximately once a week. Sampled solutions were syringe-filtered through 0.2 µm Nuclepore polycarbonate membranes and aliquots were measured for pH immediately. Of the remaining filtered supernatant, 2 ml were frozen for glucose analysis, and the remainder acidified to 1% with nitric acid for elemental analysis of Fe, Al, and Si by inductively coupled plasma–atomic emission spectrometry (ICP-AES) and ICP–mass spectrometry (ICP-MS).

After 47 days, the EPS experiments were terminated and the planchets were gently rinsed with fresh MM9 medium followed by distilled and deionized water. Planchets were then imaged using an FEI Quanta 2000 Environmental SEM operated at 5 ºC and 4.5 – 5 Torr. Following ESEM analysis, all planchets were ultrasonicated for 45 minutes in a 2% solution of sodium dodecyl sulfate (SDS), then rinsed in distilled and deionized water and ultrasonicated for 30 minutes in spectroscopic grade acetone before air-drying. SDS has been shown to effectively

remove biomatter from hornblende glass without chemically or physically altering the surfaces (Buss et al., 2003).

At the end of the bacteria-containing experiments, the bacteria in the solutions were pelleted by centrifugation, dried overnight at 65°C, and weighed.

2.2 XPS

X-ray photoelectron spectroscopy (XPS) has been used to study a variety of chemical changes at mineral surfaces such as the bioleaching of metals, leached layer formation, or adsorption of organics (e.g., Balaz et al., 1996; Blight et al., 2000; Buss et al., 2003; Hamilton et al., 2000; Kalinowski et al., 2000; Maurice et al., 2001).

Elemental concentrations of the upper ~100Å of 3 oval areas (1 x 0.7 mm each) of each of the hornblende glass planchets was analyzed by XPS using a Kratos Analytical Axis ULTRA XPS with a 1486.6 eV Al monochromatic X-ray source at 280 Watts at a takeoff angle of 90° with respect to the sample plane. The three measurements for each individual planchet were averaged. Prior to XPS analysis, samples were cleaned with spectroscopic grade acetone followed by 15 minutes of ultraviolet ozone cleaning (UVOC) to remove organic contamination (Kalinowski et al., 2000; Vig, 1992; Zazzera and Evans, 1993). Such contamination can distort elemental ratios such as Fe/Si as measured by XPS (Buss et al., 2003).

2.3 AFM

All hornblende glass planchets were imaged in air with a Digital Instruments Dimension™ 3100 Atomic Force Microscope in Tapping-Mode® (TM–AFM) using a tapping-mode etched silicon probe tip (TESP–70) at a scan-rate of 0.75 – 1.00 Hz.

Three types of images were collected of each scan, including height images, showing features both above and below the average surface level; amplitude images, showing only the positive features; and phase-contrast images, revealing variations in surface adhesive properties (Digital Instruments, 1997). Third-order plane fitting was performed on each image to eliminate tilt and S-shaped bow distortions caused by curvature of the piezoelectric stylus, thermal drift, or lateral forces (Ruppe and Duparee, 1996). Fifteen to 26 randomly chosen 100 μm^2 areas of each surface were scanned in addition to 4 – 10 μm^2 areas, which were scanned to examine surface features in detail.

The images were analyzed using Digital Instruments Nanoscope IIIa Controller software to measure the dimensions of surface features and to calculate the root mean square (RMS) roughness – the standard deviation of the height measurements relative to the basal plane – for each image. Only 100 μm^2 scans at the same resolution (39 nm lateral resolution) were compared because RMS roughness varies with scan size and resolution (e.g., Mellott et al., 2002). Fifteen RMS roughness measurements were made of the untreated, polished glass surfaces (blanks) to obtain a range of RMS roughness values for the initial variations of the glass surfaces.

2.3 *VSI*

Mirau vertical scanning interferometry (VSI) is a light-optical technique that provides an additional source of microtopographic data, providing approximately 1 nm vertical resolution in white light mode. In green light mode (i.e., a narrow band of green light centered at 550 nm), VSI has a vertical resolution of 0.7 Å. Although VSI is commonly used in industry for quality assurance applications, its use as a research tool is still relatively novel (Lasaga and Luttge,

2001; Lüttge et al., 1999). Scanning surfaces with light prevents many of the analytical artifacts that result from the physical probing involved in AFM. Additionally, VSI can scan up to a 760 x 840 μm area with a vertical scan range of up to 100 μm, while AFM scans are limited to a maximum of 90 x 90 μm with a vertical scan range of only ~ 6 μm. Although AFM suffers from pixelization, which limits resolution to the pixel size (Digital Instruments, 1997), the maximum lateral resolution of AFM (1-5 nm) is far superior to VSI (0.5-1.2 μm) making both techniques indispensable and complementary tools for analyzing surfaces in detail. A thorough description of the VSI technique is found in Lüttge et al. (1999).

A vertical scanning phase shift interferometer (MP8 8, ADE-Phase Shift, Tuscon) was used to image the hornblende glass samples. For each sample, an overall scan of 800 x 600 μm was made with a 10X objective followed by 25 scans of adjacent ~ 124 x 163 μm areas to form a 5 x 5 grid pattern using a 50X objective. The raw VSI data were analyzed using software we developed to format the data and measure RMS roughness. Topographic height images, 3-D plots, and cross-sectional traces were produced from the digitized interferograms of some scans using MAPVUE software (ADE Phase Shift, Tuscon, Arizona).

3. Results

3.1 Solution Chemistry

Concentrations of Fe in the filtered solutions, [Fe], increased with time for all conditions except those incubated with bacteria (Table 1, Figure 1a), for which [Fe] was below the lower limit of detection (0.36 μM for [Fe] by ICP-AES). Release of Fe, Al, and Si in control, xanthan-only, and alginate-only experiments was negligible (Figure 1). Release of these elements was

enhanced in all experiments containing DFAM, with alginate + DFAM experiments showing the greatest release. By day 11, xanthan + DFAM experiments showed higher [Al] and [Si], but approximately equal [Fe] compared to the DFAM-only experiments.

Throughout the experiments, changes in pH were negligible, with pH ranging from 7.2–7.6, as compared to a starting pH of 7.4. Glucose levels in abiotic experiments remained relatively constant (>1500 mg l^{-1}). Only in the experiments with bacteria were fluctuations in glucose levels observed, increasing to 600–680 mg l^{-1} immediately after replenishment with fresh medium at each sampling time point and then dropping to 4.3–6.8 mg l^{-1} by the following week. The drastic reductions in glucose levels between sampling days in the biotic solutions confirmed that the bacteria remained viable for the duration of the experiments.

3.2 Surface Chemistry

Ratios of Fe/Si on polished hornblende glass surfaces are identical within error for untreated blanks and abiotic controls incubated in medium for 39 days (Table 2, Figure 2). For our analysis, ratios are considered "unchanged" when they fall within the range of the ratios measured on the untreated blanks (Fe/Si = 0.102 – 0.110, ± 0.012). This range of values includes measurement errors of 5% for Si and 10% for Fe. This "blank range" (± 0.016) indicates sample variability and is used as an estimate of error in the XPS analyses. DFAM-only experimental surfaces have lower Fe/Si ratios (0.072 ± 0.016) than the blank range. Fe/Si ratios are significantly lower on surfaces exposed to xanthan + DFAM, whether inside or outside the dialysis bags (0.018 ± 0.016 and 0.038 ± 0.016, respectively). In contrast, Fe/Si ratios on xanthan-only experimental surfaces are unchanged. The surfaces exposed to alginate + DFAM have unchanged Fe/Si ratios regardless of the dialysis bags. The alginate-only sample incubated

289 inside the bag also has an unchanged Fe/Si ratio but the sample incubated outside the bag has an
290 elevated Fe/Si ratio (0.154 ± 0.016).
291
292 3.3 *Etch Pits*
293 No evidence for widespread adsorption of EPS on surfaces was detected by ESEM. The
294 planchet exposed to alginate-only (and not protected by dialysis tubing) did rarely contain a few
295 strands of hydrated material within some of the larger polishing scratches: such strands were not
296 observed on any other samples.
297 In AFM images, surfaces from all experiments were observed to contain polishing
298 scratches, 7-30 nm deep and < 600 nm wide as seen previously (Buss et al., 2003). All surfaces
299 also contain very small pits < 20 nm deep. However, these pits were rare (0-3 pits per 100 μm^2
300 scan) except on surfaces exposed to DFAM. Regardless of the sample treatment and pit size, etch
301 pits were roughly circular to oval-shaped. Thus, different treatments do not produce differently
302 shaped etch features as has been demonstrated for anisotropic materials such as crystals (e.g.,
303 Honess, 1929).
304 The control and EPS-only surfaces appear identical to the blanks as observed by AFM.
305 Specifically, these surfaces exhibit no distinguishable changes in the shapes or dimensions of the
306 etched polishing scratches or the bulk surfaces relative to the blanks. In contrast, some polishing
307 scratches appeared enlarged on the DFAM experiments as a result of etch pit formation along the
308 scratches (Figure 3); in addition, many etch pits were not associated with polishing scratches.
309 The DFAM-exposed surfaces also contained numerous (4–50 per 100 μm^2 area), scattered, small
310 etch pits, measuring less than 450 nm wide and less than 60 nm deep. In fact, a 100 μm^2 region

311 on any DFAM-treated planchet could not be scanned with the AFM without observing from 4 to
312 20 or more pits.

313 Etch pits on surfaces exposed to alginate + DFAM or xanthan + DFAM are comparable in
314 size and frequency to etch pits on DFAM-only surfaces regardless of dialysis tubing (Figures 3-
315 4). The glass surfaces in the EPS experiments did not show any topographic variability according
316 to presence or absence of dialysis tubing. In comparison to the DFAM-only surfaces, non-pitted
317 regions of the surfaces exposed to alginate + DFAM or xanthan + DFAM appear more corroded
318 in that the polishing features are more prominent (Figures 4-5).

319 The etch pits on the bacteria-exposed surfaces tended to be fewer (0-5 pits per 100 μm^2
320 image), larger (~300–1800 nm wide, < 95 nm deep), and grouped together, unlike those observed
321 on the DFAM experiments (Figures 3 and 6). Although etch pits also formed along the polishing
322 scratches of the surfaces that were exposed to *Bacillus* sp., these pits were too few to impact the
323 overall shape of the polishing scratches.

324

325 *3.3RMS Roughness*

326 RMS roughness, is the root-mean-square average of height deviations from the average
327 plane, calculated from the relative heights of each data point

$$RMS = \sqrt{\frac{(z_1^2 + z_2^2 + \cdots z_n^2)}{n}} \qquad (1)$$

328 where z_i is the height difference relative to the mean plane for each point *i* and *n* is the total
329 number of points measured. Fifteen AFM height images of the blanks (polished, un-treated glass
330 surfaces) were collected and analyzed for RMS roughness (Table 2, Figure 7). The range of
331 values for these blanks (2.83–5.36 nm) was used as a comparison to the glass surfaces exposed to

experimental solutions. Unusually large polishing scratches on all samples have larger RMS roughness, and were therefore avoided during imaging.

Roughness values (AFM) measured on the control, alginate-only, and xanthan-only experimental surfaces fall within the range of the blanks. All surfaces exposed to DFAM or bacteria have elevated RMS roughness as follows: (alginate + DFAM) ≈ bacteria < DFAM-only << (xanthan + DFAM). This ordering is similar to the magnitude of the surface Fe-depletion documented by XPS: (alginate + DFAM) < bacteria ≈ DFAM-only << (xanthan + DFAM). No such correlation was observed between RMS roughness and Al-depletion.

For control, bacteria, and DFAM-only surfaces, 25 adjacent 164 x 124 μm VSI scans were performed to obtain a representative analysis of the surfaces. The larger VSI scans show numerous etch pits on the DFAM-exposed surfaces (Figure 8), but due to the lower lateral resolution of the VSI scans, the majority of the DFAM-pits visible in the AFM images (< 450 nm wide) are not visible at the VSI scale. Many of the pits visible in the VSI scans may represent etching at inherent glass defects (e.g., air bubbles; Buss et al., 2003) that were avoided during AFM imaging. Rather than rely on visual analyses of these pits and other surface features, we developed algorithms to calculate RMS roughness values from the raw numerical VSI data. RMS-roughness values of the VSI images were more variable than RMS-roughness values determined on AFM images, but followed the same general trend: controls < bacteria < DFAM, confirming AFM results (Table 2).

4. Discussion

Characteristic etching and non-stoichiometric chemical changes demonstrate the coupled physical-chemical nature of microbial dissolution. It has been established that siderophores

promote mineral dissolution (Cervini-Silva and Sposito, 2002; Cheah et al., 2003; Cocozza et al., 2002; Hersman et al., 1995; Kraemer et al., 1999; Liermann et al., 2000b; Rosenberg and Maurice, 2003) and we have now shown that siderophores can alter the topography of mineral surfaces during dissolution. This is the first documented case in which the growth of etch pits in response to siderophores has been observed. Etch pits either were nucleated by siderophores or, if undetectable etch pits had previously nucleated, grew in the presence of siderophores. However, the presence of pre-existing etch pits is unlikely because the surfaces were polished prior to use in the experiments.

It has been well established that most microorganisms reside in biofilms, composed in large part by EPS, and exist attached to surfaces in natural environments (e.g., Brisou, 1995; Watnick and Kolter, 2000). Here we show that interaction of EPS with siderophores affects mineral dissolution in a manner distinct from either substance alone.

To determine the extent of dissolution, we can compare the solution chemistry, etch pits, surface roughness, and XPS data. For example, according to the solution chemistry data, release of Fe was most enhanced by alginate + DFAM. This dissolution was close to stoichiometric because the Fe/Si ratio of the surface was not changed from the blanks or controls (Figure 2). In contrast, although the solution chemistry would suggest that xanthan + DFAM experiment did not release the most Fe to solution, the surface roughness was significantly higher than for other experiements, and the Fe/Si ratio measured by XPS was significantly lower. These surface measurements indicate significant dissolution and preferential Fe release that was not evident from the solution data alone.

4.1 Surface Effects of Siderophores

Differences in size, distribution, and number of etch pits on the DFAM-exposed surfaces as compared to controls and other samples indicate that dissolution by siderophores promotes the widespread growth of etch pits on the Fe-silicate glass surfaces. Although etch pits were frequently seen along polishing scratches, the bulk surfaces (areas not marred by polishing scratches) also contained numerous pits of comparable size. Etch pits contribute to surface roughness and increased surface area, promoting further dissolution. The 240 μM concentration of DFAM used in these experiments lies within the range of siderophore concentrations estimated for soil solutions (~10 μM - mM, Hersman et al., 1995). The extensive pitting produced by DFAM under these relatively dilute conditions demonstrates the potential importance of siderophore-promoted pitting to mineral dissolution in the environment. Indeed, etch pits have been observed on hornblende crystals in the environment (e.g., Anand and Gilkes, 1984; Berner and Schott, 1982; Brantley et al., 1993; Hall and Horn, 1993; Hall and Martin, 1986; Velbel, 1989).

Dissolution stoichiometries can be documented by changes in the ratio of Fe/Si on the surfaces of the glasses. XPS evidence documents Fe depletion in the layer of glasses exposed to bacteria or DFAM alone, consistent with previous experiments with *Bacillus* sp. and hornblende crystal (Kalinowski et al., 2000) or hornblende glass (Buss et al., 2003) where Fe depletion was also shown. Lateral resolution of XPS is poor: Kalinowski et al. used a spot size of 3 mm on polished hornblende crystal and Buss et al. used a spot size of 700 μm on polished hornblende glass. XPS yields mol % elemental composition averaged over some area and depth into the surface, ~100 Å depth based upon the angle of measurement. Therefore, if the depletion observed on DFAM-only or bacteria-exposed experimental surfaces is localized to etch pits less than 2 μm wide and up to 1 μm deep, the actual depletion at the pits may be much greater than

estimated based on XPS analyses. Such a possibility has been suggested for other phases: Berner et al. (1985) proposed that localized dissolution via etch pit formation may explain apparent discrepancies between XPS-based and solution chemistry-based estimations of feldspar leached-layer thicknesses (Schott et al., 1981).

4.2 Surface Effects of EPS

Dissolution of hornblende glass (as measured by Si release, Figure 1c) was not enhanced in the presence of EPS alone. This is consistent with observations by Welch and Vandevivere (1994), who also saw no enhanced dissolution when incubating either alginate or xanthan gum with feldspars. They did observe enhanced dissolution in the presence of fresh EPS extracted from bacterial cultures in their laboratory, and proposed that low-molecular-weight metabolites present in the fresh EPS may have contributed to dissolution. Likewise, Malinovskaya et al. (1990) also found that EPS produced by *Bacillus mucilaginosus* only enhanced dissolution of silicate minerals only when incubated with minerals in combination with low molecular-weight metabolites such as organic acids. Similarly, in our experiments, EPS did not enhance release of Fe to solution without the addition of a siderophore. Welch and Vandevivere (1994) concluded that bacterial EPS may aid dissolution by affecting the affinity of reaction through complexation of dissolved cations, thereby changing the saturation state of the cation with respect to the dissolving solid.

Siderophores increase solubility by complexing aqueous Fe(III). Simulations of our experiments run using Geochemist's Workbench 4.0 (Bethke, 2002; NIST, 1998) using the thermodynamic database of Delany and Lundeen (1991) with added constants from NIST (1998) showed that our experiments were consistent with this effect. Concentrations of elements in

solution for each experiment on each sampling day were entered into the simulations. The results demonstrated that if the solution were allowed to equilibrate, control solutions (without DFAM) would precipitate iron as a ferric mineral, whereas solutions with DFAM would retain all Fe(III) as aqueous species.

In our experiments, when DFAM was added to alginate or xanthan gum, Fe release to solution more than doubled over what was observed in the presence of the siderophore alone. A similar effect was seen by Cervini-Silva and Sposito (2002) and Cheah et al. (2003) on goethite dissolution when mixing the siderophore desferrioxamine-B with oxalate. In those studies, dissolution in the presence of both the siderophore and oxalate was greater than the sum of the dissolution effects of the two ligands alone. Siderophores have significantly higher affinity for Fe(III) than does oxalate but due to their large size may be sterically hindered from forming surface complexes as easily as oxalate. Cheah et al. (2003) concluded that the siderophores in solution complexed Fe(III) from aqueous oxalate-Fe(III) complexes, freeing the oxalate ions to complex additional surface-bound Fe(III). In this way, the siderophores effectively use oxalate as an Fe shuttle.

Similarly, the presence of acetate led to an increase in the dissolution rate of amorphous Cr(III) hydroxide by each of 6 different aminocarboxylate chelators (Carbonaro, 2005). In that study, the adsorption of chelators onto the mineral surface was reduced at the same time that the dissolution rate increased. Carbonaro (2005) proposed a mechanism by which a chelator adsorbed to the Cr(III) hydroxide surface may more effectively remove a metal atom when acetate is adsorbed to a neighboring metal atom because acetate may increase the rate of ligand exchange on the bridging oxygen atom. Although acetate may not be a strong enough ligand to measurably enhance the rate of dissolution alone, in this way it may aid dissolution by other,

447 stronger, ligands such as siderophores. Carbonaro (2005) also proposed a second mechanism in
448 which the adsorption of acetate alters the speciation of adsorbed chelators. In this scenario,
449 acetate occupies neighboring coordination sites, which deters chelators from forming
450 multinuclear surface complexes in favor of mononuclear complexes, which more effectively
451 remove the metal atoms from the surface, increasing the dissolution rate.

452 In our study, we see no evidence for strong adhesion or direct physical effects from EPS-
453 surface contact in ESEM or AFM images, or in surface Fe/Si ratios. Therefore, enhanced
454 dissolution and roughness cannot be attributed to direct contact with the polymer. Xanthan gum
455 is a complex polysaccharide polymer that forms highly viscous, gel-like solutions. The primary
456 monomers of the polysaccharide backbone are D-glucose, D-mannose, and D-glucuronic acid, but
457 the polymer also contains 4.7% acetic acid and 3.0-3.5% pyruvic acid by weight (Sloneker and
458 Jeanes, 1962). The acetic acid is present as an ester (Sloneker and Jeanes, 1962), which is
459 susceptible to hydrolysis at room temperature; thus xanthan gum is likely to release acetate ions
460 into solution. Both acetate and pyruvate are small enough (60.05 and 88.06 g mol^{-1}, respectively)
461 to pass easily through the dialysis tubing (12,000-14,000 Daltons) and may have interacted with
462 the surface and enhanced siderophore-promoted dissolution via one of the aforementioned
463 mechanisms (Carbonaro, 2005; Cheah et al., 2003). Removal of Fe could de-stablilize the glass
464 structure, enhancing overall dissolution in addition to discrete dissolution at etch pits.

465 Although monodentate ligands such as acetate are not as effective at enhancing mineral
466 dissolution as multidentate ligands such as oxalate, small increases in dissolution in the presence
467 of acetate have been recorded (e.g., Hamer et al., 2003; e.g., Miller et al., 1986). In similar
468 experiments using the same MM9 medium and constant agitation (as used here), Brantley et al.
469 (2004) documented increased iron release from hornblende crystal in the presence of acetate.

To investigate the possibility of acetate release from xanthan gum and alginate in our experiments, we filtered 1-week old solutions of 0.1 g l^{-1} alginate, 0.1 g l^{-1} xanthan gum, and 240 μM DFAM, each with and without 240 μM acetic acid and analyzed them with an ion chromatograph (Dionex 2010i) using a 0.005 M Na-borate eluent and compared to a 240 μM acetic acid standard. Results were consistent with the presence of a LMWOA in solutions containing alginate or xanthan gum (as well as in all solutions spiked with acetate for comparison). Resolution of the peaks was not sufficient to positively identify acetate versus other LMWOA's. Therefore, to confirm the presence of acetate in solutions containing alginate or xanthan gum, samples of these polymers at 0.1 g l^{-1} were filtered and analyzed on a gas chromatograph mass spectrometer. Peaks were positively identified as acetate in the spectra for both polymer samples. The absence of other LMWOA's was not verified and thus other LMWOA's could have been present at much lower concentrations than acetate. However, enhanced dissolution in the presence of a siderophore and a bidentate LMWOA such as oxalate would likely be observed even at concentrations of a few micromolar oxalate (S. Kraemer, *pers. comm.*).

Exopolysaccharides from a wide variety of bacteria have been shown to contain acetyl groups, e.g., succinoglycan produced by the nitrogen-fixing soil bacterium *Sinorhizobium meliloti* (González et al., 1996), the EPS of thermophilic *Streptococcus thermophilus* (Nordmark et al., 2005), and the EPS of *Klebsiella aerogenes* (Atkins et al., 1987). Thus, siderophore-promoted dissolution enhanced by EPS-derived acetate or other small organic moieties could be an important component of biogeochemical iron cycling in a variety of bacterial biofilm systems.

Although general dissolution, as measured by Si release into solution, was enhanced by combining DFAM and xanthan gum, Fe release into solution was not enhanced over that

493 observed in the presence of DFAM alone. In contrast, Fe release was more than doubled over
494 DFAM alone when DFAM was combined with alginate. However, XPS results show the Fe/Si
495 ratio to be extremely low on the xanthan + DFAM surfaces (Figure 2), indicating either a non-
496 stoichiometric, preferential loss of Fe or precipitation of Si onto the surface. Neither of these
497 possibilities was reflected in the solution data. If some Fe were trapped within, or complexed to
498 the polymer, it may have been filtered out of the solution before ICP-MS analysis. Considering
499 the highly viscous nature of the xanthan gum in solution at 0.1 g l^{-1}, this is plausible.
500 Furthermore, trivalent metal ions including Al^{3+} and Fe^{3+} can crosslink xanthan gum inducing
501 gelation (Sabine et al., 1992), which would have increased viscosity and Fe sequestration within
502 the polymer. In addition, removal of acetyl groups from bacterial EPS has been shown to
503 increase the viscosity and crystallinity of the polymer (Atkins et al., 1987; Sutherland, 1997;
504 Sutherland, 2001), which could also restrict movement of metal ions within the polymer.
505 Elevated Fe/Si ratios on surfaces exposed directly to alginate (without DFAM) may indicate
506 back precipitation of an Fe(III)-containing phase, demonstrating a lesser tendency to sequester
507 metals compared to xanthan gum.
508
509 *4.3 Surface Effects of Bacillus sp.*
510 In experiments containing *Bacillus* sp., concentrations of Fe in solution that are below
511 detection are consistent with uptake of Fe by cells (Brantley et al., 2001). XPS data confirms
512 preferential removal of Fe from the glass surfaces exposed to bacteria (Figure 2).
513 Proton-promoted dissolution is an unlikely mechanism for etch pit formation in the
514 presence of bacteria in these experiments because 1) etch pits were not seen on control surfaces,
515 and 2) silicate dissolution should not be affected by the small pH changes observed within the

range of this study (7.2-7.6, White and Brantley, 1995). Therefore, the etch pits produced in the presence of bacteria were likely caused by ligand-promoted dissolution. Although lower pH values in microenvironments at the microbe-mineral interface can contribute to pitting (Barker and Banfield, 1998), Liermann et al. (2000a) detected a pH change of less than 0.04 across biofilms of *Bacillus* sp. grown in the same buffered medium used here in the presence of hornblende.

The production of glycocalyx by *Bacillus* sp. grown in the presence of hornblende was verified previously by Alcian Blue staining, which revealed a layer of acidic polysaccharides surrounding the cells when grown in an iron-depleted medium with hornblende crystals (Brantley et al., 2001). However, in the present experiments, *Bacillus* sp. did not produce enough polymeric material to harvest for experimentation. Iron release in the DFAM and EPS experiments cannot be directly compared to the *Bacillus* sp. experiments because these experiments contain different siderophores and EPS in different quantities. Semi-quantitative universal (Schwyn and Neilands, 1987) and catechol-specific (Arnow, 1937; Liermann et al., 2000a; Neilands and Nakamura, 1991) siderophore assays on this strain of *Bacillus* sp. growing in Fe-free MM9 medium for 3 weeks indicated approximately 180 - 200 μM catecholate siderophore in the culture solutions (B. Kalinowski, *unpublished data*). Our abiotic siderophore experiments contained 240 μM DFAM. The lower concentrations of EPS and siderophore in the *Bacillus* sp. experiments compared to the alginate+DFAM or xanthan+DFAM experiments are consistent with the trends observed in dissolution and roughness (Figure 1c and Figure 3).

The difference in size and distribution between the 'biopits' and the 'DFAM-pits' may be related to the EPS produced by the bacteria. In contrast to those produced abiotically by DFAM alone, the etch pits produced in the presence of *Bacillus* sp. are larger and more localized, often

539 forming small groups of pits (Figure 6). Additional components (besides polysaccharide) in the
540 *Bacillus* sp. EPS may have adhered more strongly to the surfaces than did alginate or xanthan
541 gum. Indeed, *Bacillus* sp. cells and cellular debris were observed by SEM and AFM,
542 respectively, on hornblende glass planchets rinsed with distilled and deionized water in our
543 previous work (Buss et al., 2003). Significant debris was not observed on planchets incubated
544 with alginate or xanthan gum, suggesting that these substances either did not adhere to the
545 surfaces or did not adhere strongly.

546 The initial step in the development of a biofilm is the adsorption of a conditioning film,
547 which may contain polysaccharides, but is thought to be primarily glycoproteins (e.g., Baier,
548 1980; Characklis, 1989). This film is dynamic, that is, constantly exchanging with solution
549 molecules, and may be heterogeneously distributed over the surface (Characklis, 1989). *Bacillus*
550 sp. likely colonized the hornblende glass surfaces by secreting a glycoprotein conditioning film
551 for the biofilm to adhere to. This film would not have formed in the alginate and xanthan gum
552 experiments.

553 Colonization-related pitting has been documented on silicate minerals before. For example,
554 in a study of natural basaltic glass, irregular localized pitting was observed after incubation for
555 181 days in seawater while the majority of the surface appeared unaltered (Thorseth et al., 1995).
556 This pitting was presumably caused by a consortia of bacteria attached to the glass surfaces that
557 were observed using SEM and TEM. Similarly, when cyanobacteria were grown on polished
558 glass, Staudigel et al. (1995) observed irregularly shaped, localized etch pits clustered along
559 zones parallel to polishing scratches. And Bennett et al. (1996a) also observed significant etching
560 in microbially colonized regions of microcline surfaces, but no etching on the uncolonized
561 regions.

562 Enzymes, molecules, and ions become concentrated in EPS, which limits their diffusion
563 into solution (Madigan et al., 2000; Morel and Palenik, 1989; Roane and Kellogg, 1996). It
564 follows that a biofilm would contain a higher concentration of siderophores than the bulk
565 solution. The viscosity of EPS may restrict movement of siderophores and other ligands; in a
566 strongly adhering biofilm, this could explain the localization of the biopits. The large biopits
567 could therefore represent assemblages of the same-sized pits as on the DFAM-exposed surfaces.
568 Therefore, EPS may be instrumental in weathering minerals because they sorb to surfaces and
569 create micro-environments with higher concentrations of ligands in close proximity to mineral
570 surfaces. Our experiments with siderophores and EPS highlight additional mechanisms by which
571 microbial communities can interact with surfaces, contributing to chemical weathering of silicate
572 minerals.

573 **5. Conclusions**

574 This study is the first to document the growth of etch pits during siderophore-promoted
575 dissolution. The widespread pitting and enhanced Fe release from siderophore-exposed surfaces
576 is consistent with chelation of Fe by siderophores, which is likely responsible for the etch pits
577 formed in the presence of *Bacillus* sp. at near-neutral pH. Small, approximately circular pits
578 formed on hornblende glass dissolved with DFAM document that siderophore-promoted
579 dissolution is localized to pits that are ubiquitous on the surface and contribute to an increase in
580 surface roughness. EPS may contribute to dissolution by providing a sink for released ions,
581 enhancing apparent solubilities; by providing additional ligands that act as Fe-shuttles for
582 siderophores; or by releasing additional ligands (such as acetate) that could alter the speciation of
583 siderophore-surface complexes or accelerate ligand exchange on surface atoms. When sorbed
584 strongly to surfaces via a conditioning film, microbial EPS may affect the size and distribution of

585 ligand-produced etch pits. Widespread pitting on siderophore-exposed surfaces demonstrates the
586 ability of siderophores to alter surface morphology. By comparison, the distribution and size of
587 microbial etch pits suggest that the 'biopits' may be caused by siderophores concentrated in
588 biofilms. Non-stoichiometric depletion of Fe on surfaces exposed to bacteria supports the
589 interpretation of localized dissolution by metal-specific ligands. Mineral surface features such as
590 etch pits provide non-exclusive evidence of microbial activity but may, when used in
591 combination with other biomarkers, provide clues to the character of microbial communities.
592

593 **Acknowledgements**

594 Funding was provided by National Science Foundation (NSF) grant EAR 00-03565,
595 Department of Energy (DOE) grant DE-FG02-01ER15209, the Penn State Biogeochemical
596 Research Initiative for Education supported by NSF-IGERT grant DGE-9972759, and the NASA
597 Astrobiology Institute Cooperative Agreement NCC2-1057. H.L. Buss acknowledges stipend
598 support of the NSF Graduate Research Fellowship Program. S.L.Brantley acknowledges support
599 from the Center for Environmental Kinetics Analysis supported by NSF grant CHE-0431328.
600 We also thank L. Liermann, A. Barnes, H. Gong, J. Kittleson, and R. Walsh for analyses and
601 laboratory assistance and S. Kraemer and R. Carbonaro for helpful discussions.
602

603 **References**

604 1997. Nanoscope Command Reference Manual, 4.3.1, Rev. B. Digital Instruments.
605 Allen, B.L. and Hajek, B.F., 1989. Mineral occurrence in soil environments. In: J.B. Dixon and
606 S.B. Weed (Editors), Minerals in Soil Environments. Soil Sci. Soc. Am., Madison, pp.
607 199-278.

608 Anand, R.R. and Gilkes, R.J., 1984. Weathering of hornblende, plagioclase and chlorite in meta-
609 dolerite, Australia. Geoderma, 34: 261-280.
610 Arnow, L.E., 1937. Colorimetric determination of the components of 3,4-
611 dihydroxyphenylalanine-tyrosine mixtures. Journal of Biological Chemistry, 118: 531-
612 537.
613 Atkins, E.D.T. et al., 1987. Effect of acetylation on the molecular interactions and gelling
614 properties of a bacterial polysaccharide. International Journal of Biological
615 Macromolecules, 9(2): 115-117.
616 Baier, R.E., 1980. Substrata influences on adhesion of microorganisms and their resultant new
617 surface properties. In: G. Bitton and K.C. Marshall (Editors), Adsorption of
618 Microorganisms to Surfaces. J. Wiley and Sons, Inc., New York, pp. 59-104.
619 Balaz, P., Kupka, D., Bastl, Z. and Achimovicova, M., 1996. Combined chemical and bacterial
620 leaching of ultrafine ground chalcopyrite. Hydrometallurgy, 42: 237-244.
621 Barker, W.W. and Banfield, J.F., 1998. Zones of Chemical and Physical Interaction at Interfaces
622 Between Microbial Communities and Minerals: A Model. Geomicrobiology, 15: 223 -
623 244.
624 Barker, W.W., Welch, S.A., Chu, S. and Banfield, J.F., 1998. Experimental Observations of the
625 Effects of Bacteria on Aluminosilicate Weathering. American Mineralogist, 83: 1551 -
626 1563.
627 Bennett, P., Hiebert, F. and Choi, W., 1996a. Microbial colonization and weathering of silicates
628 in a petroleum-contaminated groundwater. Chem Geol, 132: 45-53.
629 Bennett, P.C., Hiebert, F.K. and Choi, W.J., 1996b. Microbial colonization and weathering of
630 silicates in a petroleum-contaminated groundwater. Chemical Geology, 132: 45-53.

631 Berner, R.A., 1995. Chemical weathering and its effect on atmospheric CO_2 and climate. In: A.F.
632 White and S.L. Brantley (Editors), Chemical Weathering Rates of Silicate Minerals.
633 Reviews in Mineralogy. Mineralogical Society of America, Washington, D.C.
634 Berner, R.A., Holdren, G.R. and Schott, J., 1985. Surface layers on dissolving silicates.
635 Geochimica et Cosmochimica Acta, 49: 1657-1658.
636 Berner, R.A. and Schott, J., 1982. Mechanism of pyroxene and amphibole weathering: II.
637 Observations of soil grains. American Journal of Science, 282: 1214-1231.
638 Bethke, C.M., 2002. The Geochemists Workbench. Univ. of Illinois, Champain-Urbana, Illinois,
639 224 pp.
640 Blight, K., Ralph, D.E. and Thurgate, S., 2000. Pyrite surfaces after bio-leaching: a mechanism
641 for bio-oxidation. Hydrometallurgy, 58: 227-237.
642 Brantley, S.L., Blai, A., MacInnis, I., Cremeens, D. and Darmody, D., 1993. Natural etching
643 rates of hornblende and feldspar. Aquatic Science, 55: 262-272.
644 Brantley, S.L., Liermann, L., Bau, M. and Wu, S., 2001. Uptake of trace metals and rare earth
645 elements from hornblende by a soil bacterium. Geomicrobiology Journal, 18: 37-61.
646 Brantley, S.L. et al., 2004. Iron isotope fractionation during mineral dissolution with and without
647 bacteria. Geochimica et Cosmochimica Acta, 68(15): 3189-3204.
648 Brisou, J.F., 1995. Biofilms: Methods for enzymatic release of microorganisms. CRC Press,
649 Florida, 204 pp.
650 Budavari, S. (Editor), 1996. The Merck Index. Merck and Co., Whitehouse Stateion, N.J.
651 Buss, H.L., Brantley, S.L. and Liermann, L.J., 2003. Non-destructive methods for removal of
652 bacteria from silicate surfaces. Geomicrobiology Journal, 20(1): 25-42.

653 Buss, H.L. et al., 2005. The coupling of biological iron cycling and mineral weathering during
654 saprolite formation, Luquillo Mountains, Puerto Rico. Geobiology, 3(4): 247-260.
655 Carbonaro, R.F., 2005. Dissolution of amorphous chromium (hydr)oxide by (amino)carboxylate
656 chelating agents. Ph.D. Thesis, Johns Hopkins University, 109 pp.
657 Cervini-Silva, J. and Sposito, G., 2002. Steady-state dissolutionkinetics of aluminum-goethite in
658 the presence of desferrioxamine-B and oxalate ligands. Environ. Science and
659 Technology, 36: 337-342.
660 Characklis, W.G., 1989. Biofilm processes. In: W.G. Characklis and K.C. Marshall (Editors),
661 Biofilms. Wiley, New York, pp. 195-231.
662 Cheah, S.F., Kraemer, S.M., Cervini-Silva, J. and Sposito, G., 2003. Steady-state dissolution
663 kinetics of goethite in the presence of desferrioxamine B and oxalate ligands:
664 implications for the microbial acquisition of iron. Chemical Geology, 198: 63-75.
665 Cocozza, C. et al., 2002. Temperature dependence of goethite dissolution promoted by
666 trihydroxamate siderophores. Geochimica et Cosmochimica Acta, 66(3): 431-438.
667 Delany, J.M. and Lundeen, S.R., 1991. The LLNL Thermochemical Data Base--Revised Data
668 and File Format for the EQ3/6 Package, Yucca Mountain Site Characterization Project,
669 Department of Energy, Oak Ridge, TN.
670 Fisk, M.R., Giovannoni, S.J. and Thors`, 1998. Alteration of oceanic volcanic glass: textural
671 evidence of microbial activity. Science, 281: 978-980.
672 Furnes, H., Banerjee, N.R., Muehlenbachs, K., Staudigel, H. and de Wit, M., 2004. Early life
673 recorded in Archean pillow lavas. Science, 304: 578-581.
674 González, J.E., York, G.M. and Walker, G.C., 1996. *Rhizobium meliloti* exopolysaccharides:
675 Synthesis and symbiotic function. Gene, 179(1): 141-146.

676 Grantham, M.C. and Dove, P.M., 1996. Investigation of Bacterial-Mineral Interactions Using
677 Fluid Tapping Mode Atomic Force Microscopy. Geochimica et Cosmochimica Acta,
678 60(13): 2473 - 2480.
679 Hall, R.D. and Horn, L.L., 1993. Rates of hornblende etching in soils in glacial deposits of the
680 northern Rocky Mountains (Wyoming-Montana, USA); influence of climate and
681 characteristics of the parent material. Chemical Geology, 105: 17-29.
682 Hall, R.D. and Martin, R.F., 1986. The etching of hornblende grains in the matrix of alpine tills
683 and periglacial deposits. In: S.M. Colman and D.P. Dethier (Editors), Rates of chemical
684 weathering of rocks and minerals. Academic Press, Orlando, pp. 101-128.
685 Hamer, M., Graham, R.C., Amrhein, C. and Bozhilov, K.N., 2003. Dissolution of ripidolite (Mg,
686 Fe-Clorite) in organic and inorganic acid solutions. Soil Science Society of America
687 Journal, 67(2): 654-661.
688 Hamilton, J.P., Pantano, C.G. and Brantley, S.L., 2000. Dissolution of albite glass and crystal.
689 Geochimica et Cosmochimica Acta, 64(15): 2603-2615.
690 Hersman, L., Lloyd, T. and Sposito, G., 1995. Siderophore-promoted Dissolution of Hematite.
691 Geochimica et Cosmochimica Acta, 59(16): 3327 - 3330.
692 Hersman, L.E., 2000. The role of siderophores in iron oxide dissolution. In: D. Lovley (Editor),
693 Environmental Microbe-Metal Interactions. ASM Press, Washington, D. C., pp. 145 -
694 157.
695 Holmen, B.A. and Casey, W.H., 1996. Hydroxymate ligands, surface chemistry, and the
696 mechanism of ligand-promoted dissolution of goethite [a-FeOOH(s)]. Geochimica et
697 Cosmochimica Acta, 60: 4403-4416.

698 Honess, A.P., 1929. The theory of crystal etching and its significance in the classification of
699 crystals. Bulletin - PA State College Mineral Industries Experiment Station 3: 1-8.
700 Huang, P.M., 1989. Feldspars, olivines, pyroxenes, and amphiboles. In: J.B. Dixon and S.B.
701 Weed (Editors), Minerals in Soil Environments. Soil Sci. Soc. Am., Madison, pp. 975-
702 1050.
703 Kalinowski, B.E., Liermann, L.J., Brantley, S.L., Barnes, A. and Pantano, C.G., 2000. X-ray
704 photoelectron evidence for bacteria-enhanced dissolution of hornblende. Geochimica et
705 Cosmochimica Acta, 64(8): 1331-1343.
706 Kraemer, S.M. et al., 1999. Effect of hydroxamate siderophores on Fe release and Pb(II)
707 adsorption by goethite. Geochimica Cosmochimica Acta, 63: 3003-3008.
708 Larsen, B. and Haug, A., 1971. Biosynthesis of alginate. Part I. Composition and structure of
709 alginate produced by *Azotobacter vinelandii* (Lipman). Carbohydrate Research, 17(2):
710 287-296.
711 Lasaga, A.C. and Luttge, A., 2001. Variation of crystal dissolution rate based on a dissolution
712 stepwave model. Science, 291: 2400-2404.
713 Liermann, L.A., Barnes, A.S., Kalinowski, B.E., Zhou, X. and Brantley, S.L., 2000a.
714 Microenvironments of pH in biofilms grown on dissolving silicate surfaces. Chemical
715 Geology, 171: 1 - 6.
716 Liermann, L.J., Kalinowski, B.E., Brantley, S.L. and Ferry, J.G., 2000b. Role of bacterial
717 siderophores in dissolution of hornblende. Geochimica et Cosmochimica Acta, 64(4):
718 587-602.

719 Liermann, L.J., Marin, A., Guynn, R.L., Anbar, A. and Brantley, S.L., 2005. Production of a
720 molybdophore during metal-targeted dissolution of silicates by soil bacteria. Chemical
721 Geology: In Press.
722 Little, B.J., Wagner, P.A. and Lewandowski, Z., 1997. Spatial relationships between bacteria and
723 mineral surfaces, Geomicrobiology: Interactions Between Microbes and Minerals.
724 Reviews in mineralogy. Mineralogical Society of America, Washington, D.C., pp. 123-
725 159.
726 Lüttge, A., Bolton, E.W. and Lasaga, A.C., 1999. An interferometric study of the dissolution
727 kinetics of anorthite: The role of reactive surface area. American Journal of Science, 299:
728 652-678.
729 Lüttge, A. and Conrad, P.G., 2004. Direct observation of microbial inhibition of calcite
730 dissolution. APPLIED AND ENVIRONMENTAL MICROBIOLOGY, 70(3): 1627-
731 1632.
732 Madigan, M.T., Martinko, J.M. and Parker, J., 2000. Brock Biology of Microorganisms. Prentice
733 Hall, New Jersey, 991 pp.
734 Malinovskaya, I.M., Kosenko, L.V., Votselko, S.K. and Podgorskii, V.S., 1990. Role of Bacillus
735 mucilaginosus Polysaccharide in Degradation of Silicate Minerals. Mikrobiologiya,
736 59(1): 70 - 78.
737 Maurice, P., Forsythe, J., Hersman, L. and Sposito, G., 1996. Application of atomic-force
738 microscopy to studies of microbial interactions with hydrous Fe(III)-oxides. Chemical
739 Geology, 132: 33-43.

740 Maurice, P.A. et al., 2001. Direct observations of aluminosilicate weathering in the hyphoreic
741 zone of an Antarctic dry valley stream. Geochimica et Cosmochimica Acta, 66(8): 1335-
742 1347.
743 Medlin, J.H., Suhr, N.H. and Bodkin, J.B., 1969. Atomic absorption analysis of silicates
744 employing $LiBO_2$ fusion. Atomic Absorption Newsletter, 8(2): 25-29.
745 Mellott, N.P., Brantley, S.L. and Pantano, C.G., 2002. Topography of polished plates of albite
746 crystal and glass during dissolution. In: R. Hellmann and S.A. Wood (Editors), Water-
747 Rock Interactions, Ore Deposits, and Environmental Geochemistry: A Tribute to David
748 A. Crerar. The Geochemical Society, St. Louis, pp. 462.
749 Miller, W.P., Zelazny, L.W. and Martens, D.C., 1986. Dissolution of synthetic crystalline and
750 noncrystalline iron oxides by organic acids. Geoderma, 37(1): 1-13.
751 Morel, F.M.M. and Palenik, B., 1989. The aquatic chemistry of trace metals in biofilms. In:
752 W.G. Characklis and P.A. Wilderer (Editors), Structure and Function of Biofilms. J.
753 Wiley and Sons, New York, pp. 289-300.
754 Neilands, J.B., 1995. Siderophores: structure and function of microbial iron transport
755 compounds. Journal of Biological Chemistry, 270: 26723-26726.
756 Neilands, J.B. and Nakamura, K., 1991. Detection, determination, isolation, characterization and
757 regulation of microbial iron chelates. In: G. Winkelmann (Editor), CRC Handbook of
758 Microbial Iron Chelates. CRC Press, Boca Raton, Florida, pp. 1-14.
759 NIST, 1998. NIST Critically Selected Stability Constants of Metal Complexes Database. U.S.
760 Dept. of Commerce, Gaithersburg, MD, 42 pp.

761 Nordmark, E.L., Yang, Z., Huttunen, E. and Widmalm, G., 2005. Structrual studies of an
762 exopolysaccharide produced by *Streptococcus thermophilus* THS. Biomacromolecules, 6:
763 105-108.
764 Roane, T.M. and Kellogg, S.T., 1996. Characterization of bacterial communities in heavy metal
765 contaminated soils. Canadian Journal of Microbiology, 42: 593-603.
766 Rogers, J.R., Bennett, P.C. and Choi, W.J., 1998. Feldspars as a source of nutrients for
767 microorganisms. American Mineralogist, 83: 1532 - 1540.
768 Rohrer, J.S. and Olechno, J.D., 1992. Secondary isotope effect: The resolution of deuterated
769 glucoses by anion-exchange chromatorgaphy. Analytical Chemistry, 64: 914-916.
770 Rosenberg, D.A. and Maurice, P.A., 2003. Siderophore adsorption to and dissolution of kaolinite
771 at pH 3 to 7 and 22 C. Geochimica et Cosmochimica Acta, 67(2): 223-229.
772 Ruppe, C. and Duparee, A., 1996. Roughness analysis of optical films and substrates by atomic
773 force microscopy. Thin Solid Films, 288: 8-13.
774 Sawyer, L.K. and Hermanowicz, S.W., 1998. Detachment of biofilm bacteria due to variations in
775 nutrient supply. Water Science and Technology, 37(4-5): 211-214.
776 Schott, J., Berner, R.A. and Sjoberg, E.L., 1981. Mechanism of pyroxene and amphibole
777 weathering: I. Experimental studies of iron-free minerals. Geochimica et Cosmochimica
778 Acta, 45: 2123-2135.
779 Schwartzman, D.W. and Volk, T., 1991. Biotic enhancement of weathering and surface
780 temperatures on earth since the origin of life. Palaeogeogr. Palaeoclim. Palaeoecol., 90:
781 357-371.
782 Schwyn, B. and Neilands, J.B., 1987. Universal Chemical Assay for the Detection and
783 Determination of Siderophores. Analytical Biochemistry, 160: 47 - 56.

784 Sloneker, J.H. and Jeanes, A., 1962. Exocellular bacterial polysaccharide from Xanthomonas
785 campestris NRRL B-1459. Canadian Journal of Chemistry, 40: 2066-2071.
786 Staudigel, H., Chastain, R.A., Yayanos, A. and Bourcier, W., 1995. Biologically Mediated
787 Dissolution of Glass. Chemical Geology, 126: 147 - 154.
788 Suhr, N.H. and Ingamells, C.O., 1966. Solution technique for analysis of silicates. Analytical
789 Chemistry, 38: 730-734.
790 Sutherland, I., 1997. Microbial exopolysaccharides - structural subtleties and their consequences.
791 Pure and applied chemistry, 69(9): 1911-1917.
792 Sutherland, I.W., 2001. Biofilm exopolysaccharides: a strong and sticky framework.
793 Microbiology, 147(1): 3-9.
794 Templeton, A.S., Trainor, T.P., Spormmann, A.M. and Brown Jr., G.E., 2003. Selenium
795 speciation and partitioning within *Burkholderia cepacia* biofilms formed on α-Al_2O_3
796 surfaces. Geochimica et Cosmochimica Acta, 67(19): 3547-3557.
797 Thorseth, I.H., Furnes, H. and Tumyr, O., 1995. Textural and chemical effects of bacterial
798 activity on basaltic glass: an experimental approach. Chem. Geol., 119: 139-160.
799 Velbel, M.A., 1989. Weathering of Hornblende to Ferruginous Products by a Dissolution-
800 Reprecipitation Mechanism: Petrography and Stoichiometry. Clays and Clay Minerals,
801 37(6): 515 - 524.
802 Vig, J.R., 1992. Ultraviolet-Ozone Cleaning of Semiconductor Surfaces. Research and
803 Development Technical Report SLCET-TR-91-33, Army Research Laboratory.
804 Wang, H.-M., D., L. and Linhardt, R.J., 1991. Determination of the pK_a of glucuronic acid and
805 the carboxy groups of heparin by ^{13}C-nuclear-magnetic-resonance spectroscopy.
806 Biochemical Journal, 278: 689-695.

807 Watnick, P. and Kolter, R., 2000. Biofilm, city of microbes. Journal of Bacteriology, 182(10):
808 2675-2679.
809 Welch, S.A. and Vandevivere, P., 1994. Effect of Microbial and Other Naturally Occurring
810 Polymers on Mineral Dissolution. Geomicrobiology Journal, 12: 227 - 238.
811 White, A.F. and Brantley, S.L., 1995. Chemical weathering rates of silicate minerals: An
812 overview. In: A.F. White and S.L. Brantley (Editors), Chemical Weathering Rates of
813 Silicate Minerals. Reviews in mineralogy. Mineralogical Society of America,
814 Washington, D.C., pp. 1-22.
815 Wilderer, P.A. and Characklis, W.G., 1989. Structure and function of biofilms. In: W.G.
816 Characklis and P.A. Wilderer (Editors), Structure and Function of Biofilms. Wiley and
817 Sons, New York, pp. 5-17.
818 Winkelmann, G., 1991. Specificity of iron transport in bacteria and fungi. In: G. Winkelmann
819 (Editor), CRC Handbook of microbial iron chelates. CRC Press, Boca Raton, Florida, pp.
820 366.
821 Zazzera, L. and Evans, J.F., 1993. In situ internal reflection infrared study of aqueous
822 hydrofluoric acid and ultraviolet/ozone treated silicon (100) surfaces. Journal of Vacuum
823 Science & Technology, A11: 4934-4939.
824

825 **Figure Captions**

826 **Figure 1.** Release of Fe, Al, or Si (μM) from Fe-silicate glass surfaces to MM9 medium. **(a)** The
827 [Fe] in the bacteria-containing experiments is below the lower detection limits of the ICP-AES,
828 consistent with uptake of Fe by the bacteria. Fe release was comparable in all solutions without
829 DFAM, whereas the DFAM-containing solutions enhanced Fe release. Alginate + DFAM

solutions showed the greatest release. Similar trends are seen for **(b)** Al release and **(c)** Si release, except these elements were not completely removed from solution by the bacteria.

Figure 2. Fe/Si ratios of the upper ~100 Å of the hornblende glass surfaces measured by XPS. Error in the XPS measurements is estimated to be about 5% for Si and 10% for Fe. Measurements on replicate samples are shown as averages except for the blanks and controls, for which all replicates are shown. Sample variability is greater than the XPS measurement error for blanks: the highest and lowest Fe/Si ratios are bracketed by lines for the two blanks. This variability is used as the error on the samples. Standard deviations of the averaged values are within this variability range. The x-axis is arbitrary. Sample codes: A = alginate, X = xanthan gum, D = DFAM, B = inside dialysis bag, control = growth media only.

Figure 3. AFM height images of 10 x 10 μm areas of hornblende glass planchets. The vertical scale is ± 200 nm from the average plane (gray). Lighter and darker areas represent positive and negative topography, respectively, relative to the average plane of the surface. **(a)** Starting surfaces, or "blanks," were polished but not incubated in solution. AFM images of blanks reveal polishing scratches visible on all sample surfaces. **(b)** Control surfaces were polished and incubated in MM9 growth medium for 46 days and appear unchanged relative to blanks. **(c)** Surfaces exposed 240 μM DFAM in MM9 medium for 46 days reveal numerous, widely distributed etch pits (< 450 nm wide, < 60 nm deep). Pits were seen on un-scratched areas of the surfaces as well as along polishing scratches.

852 **Figure 4.** AFM height images of 10 x 10 μm areas of hornblende glass planchets. The vertical
853 scale is ± 200 nm from the average plane. Lighter and darker areas represent positive and
854 negative topography, respectively, relative to the average plane of the surface. **(a)** On surfaces
855 incubated in MM9 medium with xanthan gum or **(b)** alginate, polishing scratches appear slightly
856 more prominent than on control and blank surfaces (Fig. 3a-b). **(c)** When the siderophore DFAM
857 was combined with xanthan gum or **(d)** with alginate, etch pits, enlarged polishing scratches and
858 more prominently etched background texture was observed in AFM images.
859
860 **Figure 5.** Cross sections of AFM imaged surfaces exposed to **(a)** xanthan gum or **(b)** xanthan
861 gum and the siderophore DFAM. The white lines on the AFM images at the right of the figure
862 indicate the locations of the cross sections. The vertical scale is ± 50 nm.
863
864 **Figure 6. (a)** and **(b)** AFM height images of 10 x 10 μm areas of hornblende glass surfaces after
865 incubation with *Bacillus* sp. Vertical scale is ± 200 nm from the average plane, which is
866 represented by gray. Lighter and darker areas represent positive and negative topography,
867 respectively, relative to the average plane of the surface. The etch pits caused by the bacteria
868 tend to form in groups as shown here, leaving most of the surface un-pitted. Such "biopits" also
869 tend to be larger than those formed in abiotic experiments (Figs. 3-4).
870
871 **Figure 7.** Box and whisker statistical plot of root-mean-squared (RMS) roughness measured by
872 AFM on polished Fe-silicate sample surfaces. Sample codes: A = alginate, X = xanthan gum, D
873 = DFAM, B = inside dialysis bag, Bac = bacteria, Con = control (growth media only). Dotted
874 lines indicate the RMS roughness range of the untreated starting surfaces (blanks) measured on

875 15 surfaces. Boxes represent 25-75% of the data, whiskers (vertical lines) indicate 5-95% of the
876 data, X symbols bracket the range between 1 and 99% of the data and fall coincident with the
877 dash (–) symbols, which indicate the maximum and minimum values. Solid squares (■)
878 represent the mean.
879
880 **Figure 8.** VSI height image of a 164 x 124 μm area of a hornblende glass planchet incubated in
881 240 μM DFAM in MM9 growth medium. Vertical scale is ± 50 nm from the average plane. As
882 with the AFM height images, the lighter and darker areas represent positive and negative
883 topography, respectively, relative to the average plane of the surface, which is gray. The white
884 square in the bottom left corner of the image indicates the average size of the AFM scans (10 x
885 10 μm).
886

Revision for Chemical Geology

Etch pit formation on iron silicate surfaces during siderophore-promoted dissolution

Heather L. Buss[a*1], Andreas Lüttge[b], and Susan L. Brantley[c]

[a]Department of Geosciences, the Pennsylvania State University, University Park, Pennsylvania 18802 USA, hlbuss@usgs.gov

[b]Department of Earth Science MS-126, Rice University, 6100 Main Street, Houston, Texas 77005 USA, aluttge@rice.edu

[c]Earth and Environmental Systems Institute, the Pennsylvania State University, University Park, Pennsylvania 16802 USA, brantley@eesi.psu.edu

February 18, 2007

*Corresponding author, email: hlbuss@usgs.gov, tel: 650-329-4420, fax: 650-329-4538

[1]Present address: U.S. Geological Survey, Water Resources Discipline, 345 Middlefield Rd., MS 420, Menlo Park, California 94025 USA

Abstract

Understanding the effects of microbiota on mineral alteration requires the ability to recognize evidence of bacteria-promoted dissolution on mineral surfaces. Although siderophores are known to promote mineral dissolution, their effects on mineral surfaces are not well known. We have utilized atomic force microscopy (AFM), X-ray photoelectron spectroscopy (XPS), and Mirau vertical scanning interferometry (VSI) to investigate surfaces after incubation with the siderophore desferrioxamine-B mesylate (DFAM) and under colonies of bacteria. Iron-silicate glass planchets chemically similar to hornblende were incubated in buffered growth medium with siderophore-producing bacteria (*Bacillus* sp.) for 46 days with parallel abiotic experiments conducted with and without 240 μM DFAM, with and without 0.01 g l^{-1} of microbially produced extracellular polysaccharides (EPS, alginate or xanthan gum). Some glass planchets were protected by dialysis tubing from direct contact with the EPS. Weekly sampling and analysis of all filtered sample solutions showed negligible Fe and Al release in the control experiments and significant release of Fe and Al in the presence of DFAM, with negligible changes in pH. Concentration of Fe in the filtered solutions after incubation with bacteria was below detection, consistent with uptake of Fe by cells. Release of Fe, Al, and Si in control, xanthan-only, and alginate-only experiments was negligible. Release of these elements was enhanced in all experiments containing DFAM, and greatest in alginate + DFAM experiments.

AFM and VSI analyses reveal widespread, small etch pits and greater root mean squared roughness on siderophore-exposed surfaces and fewer, localized, larger etch pits on bacteria-exposed surfaces. This is the first documented case of etch pit development during siderophore-promoted dissolution. Roughness was not affected by the growth medium, alginate, or xanthan gum alone. The roughness trends among samples correlate with trends in Fe depletion

documented by XPS. Enhanced dissolution and roughness cannot be attributed to direct contact with EPS because no significant chemical or physical differences were observed between surfaces directly exposed to EPS and those protected by dialysis tubing. Acetate released from the EPS may have enhanced the siderophore-promoted dissolution. Siderophores produced by *Bacillus* sp. may be responsible for some of the 'biopits.' The difference in size and distribution of the biopits may be related to colonization.

Keywords: siderophores, etch pits, hornblende, desferrioxamine, biofilms

1. Introduction

1.1 Surface Colonization

Microbial colonization of mineral surfaces is rapid and extensive in aqueous and soil environments because organic macromolecules adsorb to surfaces and form a layer that encourages attachment of microorganisms (Baier, 1980; Brisou, 1995; Characklis, 1989; Little et al., 1997). As a result, free microorganisms represent only 0.1 to 1.0 % of total microorganisms in an aquatic ecosystem, with the remainder of the microorganisms attached to surfaces (Brisou, 1995; Madigan et al., 2000).

To colonize a surface, microorganisms form large aggregates of cells, proteins, lectins, and polysaccharides, collectively termed "biofilms" (e.g., Brisou, 1995; Little et al., 1997; e.g., Wilderer and Characklis, 1989). A number of researchers have documented the attachment of microorganisms to mineral surfaces via the formation of a biofilm (e.g., Barker et al., 1998; e.g., Thorseth et al., 1995). The nutrient content of mineral surfaces drives the attachment (Bennett et al., 1996a; Brisou, 1995; Madigan et al., 2000). In fact, in environments depleted in one or more

nutrients, microorganisms preferentially colonize mineral surfaces containing essential macro- or micronutrients (Bennett et al., 1996a; Grantham and Dove, 1996; Kalinowski et al., 2000; Rogers et al., 1998; Sawyer and Hermanowicz, 1998).

The effects of colonization on mineral surfaces remain, for the most part, un-quantified. Effects such as the formation of etch pits by microorganisms on mineral surfaces are of interest as potential biosignatures. Several researchers have documented etch pits on colonized mineral surfaces using scanning electron, transmission electron, vertical scanning interferometry or atomic force microscopies (SEM, TEM, VSI, AFM, respectively). Barker et al. (1998) and Rogers et al. (1998) saw etch pits on feldspars near attached microbial colonies. Fisk et al. (1998) observed remnants of cells within etched channels on basaltic glass collected from the sea floor and found the etchings to be consistent with microbial weathering. Similarly, Furnes et al. (2004) found tubular and segmented etchings that were likely microbial in origin on formerly glassy rims of Archean pillow basalts. Irregular etchings on hematite particles (Maurice et al., 1996) and muscovite surfaces (Maurice et al., 2001) were observed after incubation with bacteria in laboratory and field experiments, respectively. Others have documented etch pits on surfaces from which colonies have been removed (Bennett et al., 1996a; Thorseth et al., 1995). Whether the etch pits were formed by way of direct cellular attachment or chemical interactions with one or more microbial exudates is unknown. Conversely, Lüttge and Conrad (2004) found bacteria to inhibit etch pit formation on calcite surfaces.

Microorganisms produce and secrete a variety of substances that may influence mineral dissolution by lowering pH, by complexing with surface or solution ions, or by catalyzing redox reactions. Some of these substances include enzymes, alcohols, low molecular weight organic acids (LMWOA), high molecular weight extracellular polymeric substances (EPS), and highly

Fe(III)-specific ligands called siderophores. Some high affinity ligands may also be released to extract other metals (e.g., Liermann et al., 2005).

The EPS that bacteria secrete are primarily composed of glycocalyx, which are primarily polysaccharides and serve to anchor and give structure to the biofilm and to concentrate and store enzymes, ions, other bioessential molecules, and heavy metals (Brisou, 1995; Madigan et al., 2000; Morel and Palenik, 1989; Roane and Kellogg, 1996; Templeton et al., 2003).

1.2 Siderophores

Most microorganisms need ~μM concentrations of Fe to thrive (Neilands, 1995). Fe(III)-oxides (including oxides, oxyhydroxides, and hydrated oxides), specifically goethite (α-FeOOH), are the dominant forms of Fe in most aerobic soils (Hersman, 2000). Fe in these secondary minerals ultimately derives from the common rock-forming Fe-silicates: olivines, pyroxenes, amphiboles (notably hornblende), and biotite (Allen and Hajek, 1989; Huang, 1989). In soils containing these primary Fe minerals, the actions of microorganisms may affect silicate weathering rates (e.g., Bennett et al., 1996b; Buss et al., 2005; Liermann et al., 2000b) with implications for the global regulation of CO_2 over geologic timescales (e.g., Berner, 1995). However, the low solubility products of most Fe-minerals and especially Fe(III)-oxides, limit the aqueous Fe concentration at equilibrium and near-neutral pH to as low as 10^{-17} M in inorganic solutions (Schwartzman and Volk, 1991). Many microorganisms have evolved the ability to produce siderophores in order to overcome the ~10 orders of magnitude difference between available Fe and Fe needed for metabolism (Hersman, 2000).

109 Typical aqueous siderophore concentrations in nature are estimated to range from
110 approximately equal to as much as three orders of magnitude less than concentrations of
111 other chelators in soils, such as LMWOA (Hersman et al., 1995; Hersman, 2000;
112 Kalinowski et al., 2000). LMWOA can increase weathering via proton- or ligand-
113 promoted dissolution. However, siderophores have greater affinity for Fe than LMWOA
114 and previous studies have shown that siderophores are more effective than LMWOA for
115 inducing release of Fe(III) from minerals at near neutral pH (Brantley et al., 2001;
116 Holmen and Casey, 1996; Kalinowski et al., 2000).

117 Here we investigate the effects on Fe-silicate surfaces of siderophores, EPS, and
118 microorganisms that only use Fe as a micronutrient (i.e., that do not respire Fe). We
119 performed batch dissolution experiments in which flasks containing a polished Fe-silicate
120 substrate and an Fe-free, buffered, pH-neutral growth medium were each supplemented
121 with desferrioxamine-B mesylate (DFAM, the salt of a commercially available
122 siderophore) or a strain of *Bacillus* sp., an obligately aerobic soil bacterium that produces
123 an acidic glycocalyx (Brantley et al., 2001) and a catecholate siderophore (Kalinowski et
124 al., 2000). To more specifically investigate the influence of EPS on siderophore-
125 promoted dissolution, we also incubated hornblende glass planchets in batch experiments
126 with alginate or xanthan gum (Sigma), two commercially available extracellular
127 polysaccharides, with and without DFAM.

128 Surfaces were analyzed with AFM, Mirau vertical scanning interferometry (VSI), and XPS
129 to document changes in microtopography and chemistry of the surfaces. Solution analyses were
130 performed to document glucose consumption, pH changes, and Fe, Al, and Si release.

2. Materials and Methods

2.1 Experimental Setup

In order to isolate biogenic features from mineralogical features (e.g., heterogeneities among crystals, preferential dissolution of inclusions or along crystal grain boundaries), glass planchets were synthesized with a composition similar to the Fe-silicate mineral hornblende (Liermann et al., 2000a) and polished to provide a smooth, chemically analogous substrate. The composition of this "hornblende glass" (in wt%: 48.2% SiO_2, 14.5% Al_2O_3, 11.0% Fe_2O_3, 8.33% CaO, 10.9% MgO, 2.31% Na_2O, 0.51% K_2O, where Fe_2O_3 includes Fe(II) and Fe(III)) was determined using the lithium metaborate fusion technique (Medlin et al., 1969; Suhr and Ingamells, 1966) and inductively coupled plasma atomic emission spectrometry (ICP-AES). The glass was cut into planchets approximately 1 x 1 x 0.5 cm with a diamond blade and polished with diamond slurries to 0.25 μm. Polished samples were ultrasonicated in acetone for 10 minutes, air-dried, and stored in a dessicator.

The soil bacterium selected for this study was previously identified as an Arthrobacter but was subsequently found to be a *Bacillus* sp. (Buss et al., 2003). This bacterium was isolated from a hornblende-containing soil from Gore Mountain, New York, and has been shown to grow vigorously and produce siderophores in Fe-deficient growth medium in the presence of hornblende or hornblende glass (Brantley et al., 2001; Kalinowski et al., 2000; Liermann et al., 2000a). Two polished hornblende glass planchets were placed in each 500-ml glass culture flask and sterilized by autoclaving at 250°C for 20 minutes. After cooling, 150 ml of sterilized, modified iron-free MM9 medium (Liermann et al., 2000a; Schwyn and Neilands, 1987) was added aseptically. The medium composition was: 6.0 g l^{-1} Na_2HPO_4, 0.3 g l^{-1} KH_2PO_4, 0.5 g l^{-1}

NaCl, 1.0 g l^{-1} NH_4Cl, and 6.06 g l^{-1} (50 mM) TRIS buffer, prepared from ultrapure chemicals and deionized water and buffered at pH 7.4. The medium was supplemented with 2% (v/v) Chelex-100-treated 10% (w/v) casamino acids (Bio-Rad Laboratories, Difraco Laboratories, respectively), 0.2% (v/v) 1M $MgSO_4$, 1% (v/v) filter-sterilized 20% (w/v) glucose, and 0.01% (v/v) 1M $CaCl_2$, each prepared and sterilized separately. Some experiments were supplemented with filter-sterilized 240 μM DFAM, or sterilized 0.1 g ml^{-1} alginate or xanthan gum. Alginates are polysaccharides produced by several species of bacteria and algae. These polymers contain monomers of D-mannosyluronic and L-gulosyluronic acids (Budavari, 1996) or β-D-mannuronic and α-L-guluronic acids (Larsen and Haug, 1971). Xanthan gum is produced by *Xanthomonas campestris* and is composed of monomers of D-glucose, D-mannose, and D-glucuronic acid (Sloneker and Jeanes, 1962). The mannuronic acid and guluronic acid monomers of alginate have pKa's of 3.38 and 3.65, respectively and the glucose, mannose, and glucuronic acid monomers of xanthan gum have pKa's of 12.28, 12.08, and ~2.9, respectively (Rohrer and Olechno, 1992; Wang et al., 1991). The pKa's of these polymers' acid groups are below the experimental pH of 7.4 indicating that they remain deprotonated during the experiments. Although the protonation constants for DFAM are relatively high (pKa's of 8.50, 9.24, and 9.69), protonation occurs at non-chelating amino groups and thus does not interfere with Fe(III) chelation at pH values below the pKa's (Winkelmann, 1991).

Duplicate flasks for each of six conditions were set up. Abiotic conditions included 1) controls (medium + planchets), 2) DFAM-only (medium + planchets + DFAM), 3) xanthan-only (medium + planchets + xanthan gum), 4) alginate-only (medium + planchets + alginate), 4) xanthan + DFAM (medium + planchets + xanthan gum + DFAM), and 5) alginate + DFAM (medium + planchets + alginate + DFAM). To determine whether direct attachment to mineral

surfaces is required for EPS to affect dissolution, in the flasks with EPS (alginate or xanthan gum) one of the two glass planchets was enclosed in 12 – 14,000 Dalton dialysis tubing. The molecular weights of alginate and xanthan gum are about 240,000 and > 10^6 Daltons, respectively (Budavari, 1996). Thus, the dialysis tubing prevented the polymers from contacting the surfaces while permitting free flow of siderophores and other small molecules and ions. A sixth set of 2 flasks contained live bacteria (medium + planchets + 2.0 ml of an inoculum of stationary stage cultures of *Bacillus* sp.). Inocula contained 2.5 x 10^7 cells ml^{-1}, as counted on streak plates. All experiments were incubated at room temperature for 46 days on a shaker table continuously agitated at 120 rpm.

To monitor chemical changes over time and to replenish nutrients to sustain microbial growth, solutions were aseptically sampled from each flask and replaced with equivalent amounts of fresh medium ± DFAM ± EPS approximately once a week. Sampled solutions were syringe-filtered through 0.2 μm Nuclepore polycarbonate membranes and aliquots were measured for pH immediately. Of the remaining filtered supernatant, 2 ml were frozen for glucose analysis, and the remainder acidified to 1% with nitric acid for elemental analysis of Fe, Al, and Si by inductively coupled plasma–atomic emission spectrometry (ICP-AES) and ICP–mass spectrometry (ICP-MS).

After 47 days, the EPS experiments were terminated and the planchets were gently rinsed with fresh MM9 medium followed by distilled and deionized water. Planchets were then imaged using an FEI Quanta 2000 Environmental SEM operated at 5 ºC and 4.5 – 5 Torr. Following ESEM analysis, all planchets were ultrasonicated for 45 minutes in a 2% solution of sodium dodecyl sulfate (SDS), then rinsed in distilled and deionized water and ultrasonicated for 30 minutes in spectroscopic grade acetone before air-drying. SDS has been shown to effectively

remove biomatter from hornblende glass without chemically or physically altering the surfaces (Buss et al., 2003).

At the end of the bacteria-containing experiments, the bacteria in the solutions were pelleted by centrifugation, dried overnight at 65°C, and weighed.

2.2 XPS

X-ray photoelectron spectroscopy (XPS) has been used to study a variety of chemical changes at mineral surfaces such as the bioleaching of metals, leached layer formation, or adsorption of organics (e.g., Balaz et al., 1996; Blight et al., 2000; Buss et al., 2003; Hamilton et al., 2000; Kalinowski et al., 2000; Maurice et al., 2001).

Elemental concentrations of the upper ~100Å of 3 oval areas (1 x 0.7 mm each) of each of the hornblende glass planchets was analyzed by XPS using a Kratos Analytical Axis ULTRA XPS with a 1486.6 eV Al monochromatic X-ray source at 280 Watts at a takeoff angle of 90° with respect to the sample plane. The three measurements for each individual planchet were averaged. Prior to XPS analysis, samples were cleaned with spectroscopic grade acetone followed by 15 minutes of ultraviolet ozone cleaning (UVOC) to remove organic contamination (Kalinowski et al., 2000; Vig, 1992; Zazzera and Evans, 1993). Such contamination can distort elemental ratios such as Fe/Si as measured by XPS (Buss et al., 2003).

2.3 AFM

All hornblende glass planchets were imaged in air with a Digital Instruments Dimension™ 3100 Atomic Force Microscope in Tapping-Mode® (TM–AFM) using a tapping-mode etched silicon probe tip (TESP–70) at a scan-rate of 0.75 – 1.00 Hz.

Three types of images were collected of each scan, including height images, showing features both above and below the average surface level; amplitude images, showing only the positive features; and phase-contrast images, revealing variations in surface adhesive properties (Digital Instruments, 1997). Third-order plane fitting was performed on each image to eliminate tilt and S-shaped bow distortions caused by curvature of the piezoelectric stylus, thermal drift, or lateral forces (Ruppe and Duparee, 1996). Fifteen to 26 randomly chosen 100 μm^2 areas of each surface were scanned in addition to 4 – 10 μm^2 areas, which were scanned to examine surface features in detail.

The images were analyzed using Digital Instruments Nanoscope IIIa Controller software to measure the dimensions of surface features and to calculate the root mean square (RMS) roughness – the standard deviation of the height measurements relative to the basal plane – for each image. Only 100 μm^2 scans at the same resolution (39 nm lateral resolution) were compared because RMS roughness varies with scan size and resolution (e.g., Mellott et al., 2002). Fifteen RMS roughness measurements were made of the untreated, polished glass surfaces (blanks) to obtain a range of RMS roughness values for the initial variations of the glass surfaces.

2.3 *VSI*

Mirau vertical scanning interferometry (VSI) is a light-optical technique that provides an additional source of microtopographic data, providing approximately 1 nm vertical resolution in white light mode. In green light mode (i.e., a narrow band of green light centered at 550 nm), VSI has a vertical resolution of 0.7 Å. Although VSI is commonly used in industry for quality assurance applications, its use as a research tool is still relatively novel (Lasaga and Luttge,

2001; Lüttge et al., 1999). Scanning surfaces with light prevents many of the analytical artifacts that result from the physical probing involved in AFM. Additionally, VSI can scan up to a 760 x 840 μm area with a vertical scan range of up to 100 μm, while AFM scans are limited to a maximum of 90 x 90 μm with a vertical scan range of only ~ 6 μm. Although AFM suffers from pixelization, which limits resolution to the pixel size (Digital Instruments, 1997), the maximum lateral resolution of AFM (1-5 nm) is far superior to VSI (0.5-1.2 μm) making both techniques indispensable and complementary tools for analyzing surfaces in detail. A thorough description of the VSI technique is found in Lüttge et al. (1999).

A vertical scanning phase shift interferometer (MP8 8, ADE-Phase Shift, Tuscon) was used to image the hornblende glass samples. For each sample, an overall scan of 800 x 600 μm was made with a 10X objective followed by 25 scans of adjacent ~ 124 x 163 μm areas to form a 5 x 5 grid pattern using a 50X objective. The raw VSI data were analyzed using software we developed to format the data and measure RMS roughness. Topographic height images, 3-D plots, and cross-sectional traces were produced from the digitized interferograms of some scans using MAPVUE software (ADE Phase Shift, Tuscon, Arizona).

3. Results

3.1 Solution Chemistry

Concentrations of Fe in the filtered solutions, [Fe], increased with time for all conditions except those incubated with bacteria (Table 1, Figure 1a), for which [Fe] was below the lower limit of detection (0.36 μM for [Fe] by ICP-AES). Release of Fe, Al, and Si in control, xanthan-only, and alginate-only experiments was negligible (Figure 1). Release of these elements was

enhanced in all experiments containing DFAM, with alginate + DFAM experiments showing the greatest release. By day 11, xanthan + DFAM experiments showed higher [Al] and [Si], but approximately equal [Fe] compared to the DFAM-only experiments.

Throughout the experiments, changes in pH were negligible, with pH ranging from 7.2–7.6, as compared to a starting pH of 7.4. Glucose levels in abiotic experiments remained relatively constant (>1500 mg l^{-1}). Only in the experiments with bacteria were fluctuations in glucose levels observed, increasing to 600–680 mg l^{-1} immediately after replenishment with fresh medium at each sampling time point and then dropping to 4.3–6.8 mg l^{-1} by the following week. The drastic reductions in glucose levels between sampling days in the biotic solutions confirmed that the bacteria remained viable for the duration of the experiments.

3.2 Surface Chemistry

Ratios of Fe/Si on polished hornblende glass surfaces are identical within error for untreated blanks and abiotic controls incubated in medium for 39 days (Table 2, Figure 2). For our analysis, ratios are considered "unchanged" when they fall within the range of the ratios measured on the untreated blanks (Fe/Si = 0.102 – 0.110, ± 0.012). This range of values includes measurement errors of 5% for Si and 10% for Fe. This "blank range" (± 0.016) indicates sample variability and is used as an estimate of error in the XPS analyses. DFAM-only experimental surfaces have lower Fe/Si ratios (0.072 ± 0.016) than the blank range. Fe/Si ratios are significantly lower on surfaces exposed to xanthan + DFAM, whether inside or outside the dialysis bags (0.018 ± 0.016 and 0.038 ± 0.016, respectively). In contrast, Fe/Si ratios on xanthan-only experimental surfaces are unchanged. The surfaces exposed to alginate + DFAM have unchanged Fe/Si ratios regardless of the dialysis bags. The alginate-only sample incubated

289 inside the bag also has an unchanged Fe/Si ratio but the sample incubated outside the bag has an
290 elevated Fe/Si ratio (0.154 ± 0.016).
291
292 3.3 *Etch Pits*
293 No evidence for widespread adsorption of EPS on surfaces was detected by ESEM. The
294 planchet exposed to alginate-only (and not protected by dialysis tubing) did rarely contain a few
295 strands of hydrated material within some of the larger polishing scratches: such strands were not
296 observed on any other samples.
297 In AFM images, surfaces from all experiments were observed to contain polishing
298 scratches, 7-30 nm deep and < 600 nm wide as seen previously (Buss et al., 2003). All surfaces
299 also contain very small pits < 20 nm deep. However, these pits were rare (0-3 pits per 100 μm^2
300 scan) except on surfaces exposed to DFAM. Regardless of the sample treatment and pit size, etch
301 pits were roughly circular to oval-shaped. Thus, different treatments do not produce differently
302 shaped etch features as has been demonstrated for anisotropic materials such as crystals (e.g.,
303 Honess, 1929).
304 The control and EPS-only surfaces appear identical to the blanks as observed by AFM.
305 Specifically, these surfaces exhibit no distinguishable changes in the shapes or dimensions of the
306 etched polishing scratches or the bulk surfaces relative to the blanks. In contrast, some polishing
307 scratches appeared enlarged on the DFAM experiments as a result of etch pit formation along the
308 scratches (Figure 3); in addition, many etch pits were not associated with polishing scratches.
309 The DFAM-exposed surfaces also contained numerous (4–50 per 100 μm^2 area), scattered, small
310 etch pits, measuring less than 450 nm wide and less than 60 nm deep. In fact, a 100 μm^2 region

311 on any DFAM-treated planchet could not be scanned with the AFM without observing from 4 to
312 20 or more pits.

313 Etch pits on surfaces exposed to alginate + DFAM or xanthan + DFAM are comparable in
314 size and frequency to etch pits on DFAM-only surfaces regardless of dialysis tubing (Figures 3-
315 4). The glass surfaces in the EPS experiments did not show any topographic variability according
316 to presence or absence of dialysis tubing. In comparison to the DFAM-only surfaces, non-pitted
317 regions of the surfaces exposed to alginate + DFAM or xanthan + DFAM appear more corroded
318 in that the polishing features are more prominent (Figures 4-5).

319 The etch pits on the bacteria-exposed surfaces tended to be fewer (0-5 pits per 100 μm^2
320 image), larger (~300–1800 nm wide, < 95 nm deep), and grouped together, unlike those observed
321 on the DFAM experiments (Figures 3 and 6). Although etch pits also formed along the polishing
322 scratches of the surfaces that were exposed to *Bacillus* sp., these pits were too few to impact the
323 overall shape of the polishing scratches.

324

325 *3.3RMS Roughness*

326 RMS roughness, is the root-mean-square average of height deviations from the average
327 plane, calculated from the relative heights of each data point

$$RMS = \sqrt{\frac{(z_1^2 + z_2^2 + \cdots z_n^2)}{n}} \quad (1)$$

328 where z_i is the height difference relative to the mean plane for each point *i* and *n* is the total
329 number of points measured. Fifteen AFM height images of the blanks (polished, un-treated glass
330 surfaces) were collected and analyzed for RMS roughness (Table 2, Figure 7). The range of
331 values for these blanks (2.83–5.36 nm) was used as a comparison to the glass surfaces exposed to

experimental solutions. Unusually large polishing scratches on all samples have larger RMS roughness, and were therefore avoided during imaging.

Roughness values (AFM) measured on the control, alginate-only, and xanthan-only experimental surfaces fall within the range of the blanks. All surfaces exposed to DFAM or bacteria have elevated RMS roughness as follows: (alginate + DFAM) ≈ bacteria < DFAM-only << (xanthan + DFAM). This ordering is similar to the magnitude of the surface Fe-depletion documented by XPS: (alginate + DFAM) < bacteria ≈ DFAM-only << (xanthan + DFAM). No such correlation was observed between RMS roughness and Al-depletion.

For control, bacteria, and DFAM-only surfaces, 25 adjacent 164 x 124 μm VSI scans were performed to obtain a representative analysis of the surfaces. The larger VSI scans show numerous etch pits on the DFAM-exposed surfaces (Figure 8), but due to the lower lateral resolution of the VSI scans, the majority of the DFAM-pits visible in the AFM images (< 450 nm wide) are not visible at the VSI scale. Many of the pits visible in the VSI scans may represent etching at inherent glass defects (e.g., air bubbles; Buss et al., 2003) that were avoided during AFM imaging. Rather than rely on visual analyses of these pits and other surface features, we developed algorithms to calculate RMS roughness values from the raw numerical VSI data. RMS-roughness values of the VSI images were more variable than RMS-roughness values determined on AFM images, but followed the same general trend: controls < bacteria < DFAM, confirming AFM results (Table 2).

4. Discussion

Characteristic etching and non-stoichiometric chemical changes demonstrate the coupled physical-chemical nature of microbial dissolution. It has been established that siderophores

promote mineral dissolution (Cervini-Silva and Sposito, 2002; Cheah et al., 2003; Cocozza et al., 2002; Hersman et al., 1995; Kraemer et al., 1999; Liermann et al., 2000b; Rosenberg and Maurice, 2003) and we have now shown that siderophores can alter the topography of mineral surfaces during dissolution. This is the first documented case in which the growth of etch pits in response to siderophores has been observed. Etch pits either were nucleated by siderophores or, if undetectable etch pits had previously nucleated, grew in the presence of siderophores. However, the presence of pre-existing etch pits is unlikely because the surfaces were polished prior to use in the experiments.

It has been well established that most microorganisms reside in biofilms, composed in large part by EPS, and exist attached to surfaces in natural environments (e.g., Brisou, 1995; Watnick and Kolter, 2000). Here we show that interaction of EPS with siderophores affects mineral dissolution in a manner distinct from either substance alone.

To determine the extent of dissolution, we can compare the solution chemistry, etch pits, surface roughness, and XPS data. For example, according to the solution chemistry data, release of Fe was most enhanced by alginate + DFAM. This dissolution was close to stoichiometric because the Fe/Si ratio of the surface was not changed from the blanks or controls (Figure 2). In contrast, although the solution chemistry would suggest that xanthan + DFAM experiment did not release the most Fe to solution, the surface roughness was significantly higher than for other experiements, and the Fe/Si ratio measured by XPS was significantly lower. These surface measurements indicate significant dissolution and preferential Fe release that was not evident from the solution data alone.

4.1 Surface Effects of Siderophores

Differences in size, distribution, and number of etch pits on the DFAM-exposed surfaces as compared to controls and other samples indicate that dissolution by siderophores promotes the widespread growth of etch pits on the Fe-silicate glass surfaces. Although etch pits were frequently seen along polishing scratches, the bulk surfaces (areas not marred by polishing scratches) also contained numerous pits of comparable size. Etch pits contribute to surface roughness and increased surface area, promoting further dissolution. The 240 μM concentration of DFAM used in these experiments lies within the range of siderophore concentrations estimated for soil solutions (~10 μM - mM, Hersman et al., 1995). The extensive pitting produced by DFAM under these relatively dilute conditions demonstrates the potential importance of siderophore-promoted pitting to mineral dissolution in the environment. Indeed, etch pits have been observed on hornblende crystals in the environment (e.g., Anand and Gilkes, 1984; Berner and Schott, 1982; Brantley et al., 1993; Hall and Horn, 1993; Hall and Martin, 1986; Velbel, 1989).

Dissolution stoichiometries can be documented by changes in the ratio of Fe/Si on the surfaces of the glasses. XPS evidence documents Fe depletion in the layer of glasses exposed to bacteria or DFAM alone, consistent with previous experiments with *Bacillus* sp. and hornblende crystal (Kalinowski et al., 2000) or hornblende glass (Buss et al., 2003) where Fe depletion was also shown. Lateral resolution of XPS is poor: Kalinowski et al. used a spot size of 3 mm on polished hornblende crystal and Buss et al. used a spot size of 700 μm on polished hornblende glass. XPS yields mol % elemental composition averaged over some area and depth into the surface, ~100 Å depth based upon the angle of measurement. Therefore, if the depletion observed on DFAM-only or bacteria-exposed experimental surfaces is localized to etch pits less than 2 μm wide and up to 1 μm deep, the actual depletion at the pits may be much greater than

estimated based on XPS analyses. Such a possibility has been suggested for other phases: Berner et al. (1985) proposed that localized dissolution via etch pit formation may explain apparent discrepancies between XPS-based and solution chemistry-based estimations of feldspar leached-layer thicknesses (Schott et al., 1981).

4.2 Surface Effects of EPS

Dissolution of hornblende glass (as measured by Si release, Figure 1c) was not enhanced in the presence of EPS alone. This is consistent with observations by Welch and Vandevivere (1994), who also saw no enhanced dissolution when incubating either alginate or xanthan gum with feldspars. They did observe enhanced dissolution in the presence of fresh EPS extracted from bacterial cultures in their laboratory, and proposed that low-molecular-weight metabolites present in the fresh EPS may have contributed to dissolution. Likewise, Malinovskaya et al. (1990) also found that EPS produced by *Bacillus mucilaginosus* only enhanced dissolution of silicate minerals only when incubated with minerals in combination with low molecular-weight metabolites such as organic acids. Similarly, in our experiments, EPS did not enhance release of Fe to solution without the addition of a siderophore. Welch and Vandevivere (1994) concluded that bacterial EPS may aid dissolution by affecting the affinity of reaction through complexation of dissolved cations, thereby changing the saturation state of the cation with respect to the dissolving solid.

Siderophores increase solubility by complexing aqueous Fe(III). Simulations of our experiments run using Geochemist's Workbench 4.0 (Bethke, 2002; NIST, 1998) using the thermodynamic database of Delany and Lundeen (1991) with added constants from NIST (1998) showed that our experiments were consistent with this effect. Concentrations of elements in

solution for each experiment on each sampling day were entered into the simulations. The results demonstrated that if the solution were allowed to equilibrate, control solutions (without DFAM) would precipitate iron as a ferric mineral, whereas solutions with DFAM would retain all Fe(III) as aqueous species.

In our experiments, when DFAM was added to alginate or xanthan gum, Fe release to solution more than doubled over what was observed in the presence of the siderophore alone. A similar effect was seen by Cervini-Silva and Sposito (2002) and Cheah et al. (2003) on goethite dissolution when mixing the siderophore desferrioxamine-B with oxalate. In those studies, dissolution in the presence of both the siderophore and oxalate was greater than the sum of the dissolution effects of the two ligands alone. Siderophores have significantly higher affinity for Fe(III) than does oxalate but due to their large size may be sterically hindered from forming surface complexes as easily as oxalate. Cheah et al. (2003) concluded that the siderophores in solution complexed Fe(III) from aqueous oxalate-Fe(III) complexes, freeing the oxalate ions to complex additional surface-bound Fe(III). In this way, the siderophores effectively use oxalate as an Fe shuttle.

Similarly, the presence of acetate led to an increase in the dissolution rate of amorphous Cr(III) hydroxide by each of 6 different aminocarboxylate chelators (Carbonaro, 2005). In that study, the adsorption of chelators onto the mineral surface was reduced at the same time that the dissolution rate increased. Carbonaro (2005) proposed a mechanism by which a chelator adsorbed to the Cr(III) hydroxide surface may more effectively remove a metal atom when acetate is adsorbed to a neighboring metal atom because acetate may increase the rate of ligand exchange on the bridging oxygen atom. Although acetate may not be a strong enough ligand to measurably enhance the rate of dissolution alone, in this way it may aid dissolution by other,

447 stronger, ligands such as siderophores. Carbonaro (2005) also proposed a second mechanism in
448 which the adsorption of acetate alters the speciation of adsorbed chelators. In this scenario,
449 acetate occupies neighboring coordination sites, which deters chelators from forming
450 multinuclear surface complexes in favor of mononuclear complexes, which more effectively
451 remove the metal atoms from the surface, increasing the dissolution rate.

452 In our study, we see no evidence for strong adhesion or direct physical effects from EPS-
453 surface contact in ESEM or AFM images, or in surface Fe/Si ratios. Therefore, enhanced
454 dissolution and roughness cannot be attributed to direct contact with the polymer. Xanthan gum
455 is a complex polysaccharide polymer that forms highly viscous, gel-like solutions. The primary
456 monomers of the polysaccharide backbone are D-glucose, D-mannose, and D-glucuronic acid, but
457 the polymer also contains 4.7% acetic acid and 3.0-3.5% pyruvic acid by weight (Sloneker and
458 Jeanes, 1962). The acetic acid is present as an ester (Sloneker and Jeanes, 1962), which is
459 susceptible to hydrolysis at room temperature; thus xanthan gum is likely to release acetate ions
460 into solution. Both acetate and pyruvate are small enough (60.05 and 88.06 g mol^{-1}, respectively)
461 to pass easily through the dialysis tubing (12,000-14,000 Daltons) and may have interacted with
462 the surface and enhanced siderophore-promoted dissolution via one of the aforementioned
463 mechanisms (Carbonaro, 2005; Cheah et al., 2003). Removal of Fe could de-stablilize the glass
464 structure, enhancing overall dissolution in addition to discrete dissolution at etch pits.

465 Although monodentate ligands such as acetate are not as effective at enhancing mineral
466 dissolution as multidentate ligands such as oxalate, small increases in dissolution in the presence
467 of acetate have been recorded (e.g., Hamer et al., 2003; e.g., Miller et al., 1986). In similar
468 experiments using the same MM9 medium and constant agitation (as used here), Brantley et al.
469 (2004) documented increased iron release from hornblende crystal in the presence of acetate.

To investigate the possibility of acetate release from xanthan gum and alginate in our experiments, we filtered 1-week old solutions of 0.1 g l^{-1} alginate, 0.1 g l^{-1} xanthan gum, and 240 μM DFAM, each with and without 240 μM acetic acid and analyzed them with an ion chromatograph (Dionex 2010i) using a 0.005 M Na-borate eluent and compared to a 240 μM acetic acid standard. Results were consistent with the presence of a LMWOA in solutions containing alginate or xanthan gum (as well as in all solutions spiked with acetate for comparison). Resolution of the peaks was not sufficient to positively identify acetate versus other LMWOA's. Therefore, to confirm the presence of acetate in solutions containing alginate or xanthan gum, samples of these polymers at 0.1 g l^{-1} were filtered and analyzed on a gas chromatograph mass spectrometer. Peaks were positively identified as acetate in the spectra for both polymer samples. The absence of other LMWOA's was not verified and thus other LMWOA's could have been present at much lower concentrations than acetate. However, enhanced dissolution in the presence of a siderophore and a bidentate LMWOA such as oxalate would likely be observed even at concentrations of a few micromolar oxalate (S. Kraemer, *pers. comm.*).

Exopolysaccharides from a wide variety of bacteria have been shown to contain acetyl groups, e.g., succinoglycan produced by the nitrogen-fixing soil bacterium *Sinorhizobium meliloti* (González et al., 1996), the EPS of thermophilic *Streptococcus thermophilus* (Nordmark et al., 2005), and the EPS of *Klebsiella aerogenes* (Atkins et al., 1987). Thus, siderophore-promoted dissolution enhanced by EPS-derived acetate or other small organic moieties could be an important component of biogeochemical iron cycling in a variety of bacterial biofilm systems.

Although general dissolution, as measured by Si release into solution, was enhanced by combining DFAM and xanthan gum, Fe release into solution was not enhanced over that

493 observed in the presence of DFAM alone. In contrast, Fe release was more than doubled over
494 DFAM alone when DFAM was combined with alginate. However, XPS results show the Fe/Si
495 ratio to be extremely low on the xanthan + DFAM surfaces (Figure 2), indicating either a non-
496 stoichiometric, preferential loss of Fe or precipitation of Si onto the surface. Neither of these
497 possibilities was reflected in the solution data. If some Fe were trapped within, or complexed to
498 the polymer, it may have been filtered out of the solution before ICP-MS analysis. Considering
499 the highly viscous nature of the xanthan gum in solution at 0.1 g l^{-1}, this is plausible.
500 Furthermore, trivalent metal ions including Al^{3+} and Fe^{3+} can crosslink xanthan gum inducing
501 gelation (Sabine et al., 1992), which would have increased viscosity and Fe sequestration within
502 the polymer. In addition, removal of acetyl groups from bacterial EPS has been shown to
503 increase the viscosity and crystallinity of the polymer (Atkins et al., 1987; Sutherland, 1997;
504 Sutherland, 2001), which could also restrict movement of metal ions within the polymer.
505 Elevated Fe/Si ratios on surfaces exposed directly to alginate (without DFAM) may indicate
506 back precipitation of an Fe(III)-containing phase, demonstrating a lesser tendency to sequester
507 metals compared to xanthan gum.
508
509 *4.3 Surface Effects of Bacillus sp.*
510 In experiments containing *Bacillus* sp., concentrations of Fe in solution that are below
511 detection are consistent with uptake of Fe by cells (Brantley et al., 2001). XPS data confirms
512 preferential removal of Fe from the glass surfaces exposed to bacteria (Figure 2).
513 Proton-promoted dissolution is an unlikely mechanism for etch pit formation in the
514 presence of bacteria in these experiments because 1) etch pits were not seen on control surfaces,
515 and 2) silicate dissolution should not be affected by the small pH changes observed within the

range of this study (7.2-7.6, White and Brantley, 1995). Therefore, the etch pits produced in the presence of bacteria were likely caused by ligand-promoted dissolution. Although lower pH values in microenvironments at the microbe-mineral interface can contribute to pitting (Barker and Banfield, 1998), Liermann et al. (2000a) detected a pH change of less than 0.04 across biofilms of *Bacillus* sp. grown in the same buffered medium used here in the presence of hornblende.

The production of glycocalyx by *Bacillus* sp. grown in the presence of hornblende was verified previously by Alcian Blue staining, which revealed a layer of acidic polysaccharides surrounding the cells when grown in an iron-depleted medium with hornblende crystals (Brantley et al., 2001). However, in the present experiments, *Bacillus* sp. did not produce enough polymeric material to harvest for experimentation. Iron release in the DFAM and EPS experiments cannot be directly compared to the *Bacillus* sp. experiments because these experiments contain different siderophores and EPS in different quantities. Semi-quantitative universal (Schwyn and Neilands, 1987) and catechol-specific (Arnow, 1937; Liermann et al., 2000a; Neilands and Nakamura, 1991) siderophore assays on this strain of *Bacillus* sp. growing in Fe-free MM9 medium for 3 weeks indicated approximately 180 - 200 μM catecholate siderophore in the culture solutions (B. Kalinowski, *unpublished data*). Our abiotic siderophore experiments contained 240 μM DFAM. The lower concentrations of EPS and siderophore in the *Bacillus* sp. experiments compared to the alginate+DFAM or xanthan+DFAM experiments are consistent with the trends observed in dissolution and roughness (Figure 1c and Figure 3).

The difference in size and distribution between the 'biopits' and the 'DFAM-pits' may be related to the EPS produced by the bacteria. In contrast to those produced abiotically by DFAM alone, the etch pits produced in the presence of *Bacillus* sp. are larger and more localized, often

539 forming small groups of pits (Figure 6). Additional components (besides polysaccharide) in the
540 *Bacillus* sp. EPS may have adhered more strongly to the surfaces than did alginate or xanthan
541 gum. Indeed, *Bacillus* sp. cells and cellular debris were observed by SEM and AFM,
542 respectively, on hornblende glass planchets rinsed with distilled and deionized water in our
543 previous work (Buss et al., 2003). Significant debris was not observed on planchets incubated
544 with alginate or xanthan gum, suggesting that these substances either did not adhere to the
545 surfaces or did not adhere strongly.

546 The initial step in the development of a biofilm is the adsorption of a conditioning film,
547 which may contain polysaccharides, but is thought to be primarily glycoproteins (e.g., Baier,
548 1980; Characklis, 1989). This film is dynamic, that is, constantly exchanging with solution
549 molecules, and may be heterogeneously distributed over the surface (Characklis, 1989). *Bacillus*
550 sp. likely colonized the hornblende glass surfaces by secreting a glycoprotein conditioning film
551 for the biofilm to adhere to. This film would not have formed in the alginate and xanthan gum
552 experiments.

553 Colonization-related pitting has been documented on silicate minerals before. For example,
554 in a study of natural basaltic glass, irregular localized pitting was observed after incubation for
555 181 days in seawater while the majority of the surface appeared unaltered (Thorseth et al., 1995).
556 This pitting was presumably caused by a consortia of bacteria attached to the glass surfaces that
557 were observed using SEM and TEM. Similarly, when cyanobacteria were grown on polished
558 glass, Staudigel et al. (1995) observed irregularly shaped, localized etch pits clustered along
559 zones parallel to polishing scratches. And Bennett et al. (1996a) also observed significant etching
560 in microbially colonized regions of microcline surfaces, but no etching on the uncolonized
561 regions.

Enzymes, molecules, and ions become concentrated in EPS, which limits their diffusion into solution (Madigan et al., 2000; Morel and Palenik, 1989; Roane and Kellogg, 1996). It follows that a biofilm would contain a higher concentration of siderophores than the bulk solution. The viscosity of EPS may restrict movement of siderophores and other ligands; in a strongly adhering biofilm, this could explain the localization of the biopits. The large biopits could therefore represent assemblages of the same-sized pits as on the DFAM-exposed surfaces. Therefore, EPS may be instrumental in weathering minerals because they sorb to surfaces and create micro-environments with higher concentrations of ligands in close proximity to mineral surfaces. Our experiments with siderophores and EPS highlight additional mechanisms by which microbial communities can interact with surfaces, contributing to chemical weathering of silicate minerals.

5. Conclusions

This study is the first to document the growth of etch pits during siderophore-promoted dissolution. The widespread pitting and enhanced Fe release from siderophore-exposed surfaces is consistent with chelation of Fe by siderophores, which is likely responsible for the etch pits formed in the presence of *Bacillus* sp. at near-neutral pH. Small, approximately circular pits formed on hornblende glass dissolved with DFAM document that siderophore-promoted dissolution is localized to pits that are ubiquitous on the surface and contribute to an increase in surface roughness. EPS may contribute to dissolution by providing a sink for released ions, enhancing apparent solubilities; by providing additional ligands that act as Fe-shuttles for siderophores; or by releasing additional ligands (such as acetate) that could alter the speciation of siderophore-surface complexes or accelerate ligand exchange on surface atoms. When sorbed strongly to surfaces via a conditioning film, microbial EPS may affect the size and distribution of

585 ligand-produced etch pits. Widespread pitting on siderophore-exposed surfaces demonstrates the
586 ability of siderophores to alter surface morphology. By comparison, the distribution and size of
587 microbial etch pits suggest that the 'biopits' may be caused by siderophores concentrated in
588 biofilms. Non-stoichiometric depletion of Fe on surfaces exposed to bacteria supports the
589 interpretation of localized dissolution by metal-specific ligands. Mineral surface features such as
590 etch pits provide non-exclusive evidence of microbial activity but may, when used in
591 combination with other biomarkers, provide clues to the character of microbial communities.
592

593 **Acknowledgements**

594 Funding was provided by National Science Foundation (NSF) grant EAR 00-03565,
595 Department of Energy (DOE) grant DE-FG02-01ER15209, the Penn State Biogeochemical
596 Research Initiative for Education supported by NSF-IGERT grant DGE-9972759, and the NASA
597 Astrobiology Institute Cooperative Agreement NCC2-1057. H.L. Buss acknowledges stipend
598 support of the NSF Graduate Research Fellowship Program. S.L.Brantley acknowledges support
599 from the Center for Environmental Kinetics Analysis supported by NSF grant CHE-0431328.
600 We also thank L. Liermann, A. Barnes, H. Gong, J. Kittleson, and R. Walsh for analyses and
601 laboratory assistance and S. Kraemer and R. Carbonaro for helpful discussions.
602

603 **References**

604 1997. Nanoscope Command Reference Manual, 4.3.1, Rev. B. Digital Instruments.
605 Allen, B.L. and Hajek, B.F., 1989. Mineral occurrence in soil environments. In: J.B. Dixon and
606 S.B. Weed (Editors), Minerals in Soil Environments. Soil Sci. Soc. Am., Madison, pp.
607 199-278.

608 Anand, R.R. and Gilkes, R.J., 1984. Weathering of hornblende, plagioclase and chlorite in meta-
609 dolerite, Australia. Geoderma, 34: 261-280.
610 Arnow, L.E., 1937. Colorimetric determination of the components of 3,4-
611 dihydroxyphenylalanine-tyrosine mixtures. Journal of Biological Chemistry, 118: 531-
612 537.
613 Atkins, E.D.T. et al., 1987. Effect of acetylation on the molecular interactions and gelling
614 properties of a bacterial polysaccharide. International Journal of Biological
615 Macromolecules, 9(2): 115-117.
616 Baier, R.E., 1980. Substrata influences on adhesion of microorganisms and their resultant new
617 surface properties. In: G. Bitton and K.C. Marshall (Editors), Adsorption of
618 Microorganisms to Surfaces. J. Wiley and Sons, Inc., New York, pp. 59-104.
619 Balaz, P., Kupka, D., Bastl, Z. and Achimovicova, M., 1996. Combined chemical and bacterial
620 leaching of ultrafine ground chalcopyrite. Hydrometallurgy, 42: 237-244.
621 Barker, W.W. and Banfield, J.F., 1998. Zones of Chemical and Physical Interaction at Interfaces
622 Between Microbial Communities and Minerals: A Model. Geomicrobiology, 15: 223 -
623 244.
624 Barker, W.W., Welch, S.A., Chu, S. and Banfield, J.F., 1998. Experimental Observations of the
625 Effects of Bacteria on Aluminosilicate Weathering. American Mineralogist, 83: 1551 -
626 1563.
627 Bennett, P., Hiebert, F. and Choi, W., 1996a. Microbial colonization and weathering of silicates
628 in a petroleum-contaminated groundwater. Chem Geol, 132: 45-53.
629 Bennett, P.C., Hiebert, F.K. and Choi, W.J., 1996b. Microbial colonization and weathering of
630 silicates in a petroleum-contaminated groundwater. Chemical Geology, 132: 45-53.

631 Berner, R.A., 1995. Chemical weathering and its effect on atmospheric CO_2 and climate. In: A.F.
632 White and S.L. Brantley (Editors), Chemical Weathering Rates of Silicate Minerals.
633 Reviews in Mineralogy. Mineralogical Society of America, Washington, D.C.
634 Berner, R.A., Holdren, G.R. and Schott, J., 1985. Surface layers on dissolving silicates.
635 Geochimica et Cosmochimica Acta, 49: 1657-1658.
636 Berner, R.A. and Schott, J., 1982. Mechanism of pyroxene and amphibole weathering: II.
637 Observations of soil grains. American Journal of Science, 282: 1214-1231.
638 Bethke, C.M., 2002. The Geochemists Workbench. Univ. of Illinois, Champain-Urbana, Illinois,
639 224 pp.
640 Blight, K., Ralph, D.E. and Thurgate, S., 2000. Pyrite surfaces after bio-leaching: a mechanism
641 for bio-oxidation. Hydrometallurgy, 58: 227-237.
642 Brantley, S.L., Blai, A., MacInnis, I., Cremeens, D. and Darmody, D., 1993. Natural etching
643 rates of hornblende and feldspar. Aquatic Science, 55: 262-272.
644 Brantley, S.L., Liermann, L., Bau, M. and Wu, S., 2001. Uptake of trace metals and rare earth
645 elements from hornblende by a soil bacterium. Geomicrobiology Journal, 18: 37-61.
646 Brantley, S.L. et al., 2004. Iron isotope fractionation during mineral dissolution with and without
647 bacteria. Geochimica et Cosmochimica Acta, 68(15): 3189-3204.
648 Brisou, J.F., 1995. Biofilms: Methods for enzymatic release of microorganisms. CRC Press,
649 Florida, 204 pp.
650 Budavari, S. (Editor), 1996. The Merck Index. Merck and Co., Whitehouse Stateion, N.J.
651 Buss, H.L., Brantley, S.L. and Liermann, L.J., 2003. Non-destructive methods for removal of
652 bacteria from silicate surfaces. Geomicrobiology Journal, 20(1): 25-42.

653 Buss, H.L. et al., 2005. The coupling of biological iron cycling and mineral weathering during
654 saprolite formation, Luquillo Mountains, Puerto Rico. Geobiology, 3(4): 247-260.
655 Carbonaro, R.F., 2005. Dissolution of amorphous chromium (hydr)oxide by (amino)carboxylate
656 chelating agents. Ph.D. Thesis, Johns Hopkins University, 109 pp.
657 Cervini-Silva, J. and Sposito, G., 2002. Steady-state dissolutionkinetics of aluminum-goethite in
658 the presence of desferrioxamine-B and oxalate ligands. Environ. Science and
659 Technology, 36: 337-342.
660 Characklis, W.G., 1989. Biofilm processes. In: W.G. Characklis and K.C. Marshall (Editors),
661 Biofilms. Wiley, New York, pp. 195-231.
662 Cheah, S.F., Kraemer, S.M., Cervini-Silva, J. and Sposito, G., 2003. Steady-state dissolution
663 kinetics of goethite in the presence of desferrioxamine B and oxalate ligands:
664 implications for the microbial acquisition of iron. Chemical Geology, 198: 63-75.
665 Cocozza, C. et al., 2002. Temperature dependence of goethite dissolution promoted by
666 trihydroxamate siderophores. Geochimica et Cosmochimica Acta, 66(3): 431-438.
667 Delany, J.M. and Lundeen, S.R., 1991. The LLNL Thermochemical Data Base--Revised Data
668 and File Format for the EQ3/6 Package, Yucca Mountain Site Characterization Project,
669 Department of Energy, Oak Ridge, TN.
670 Fisk, M.R., Giovannoni, S.J. and Thors`, 1998. Alteration of oceanic volcanic glass: textural
671 evidence of microbial activity. Science, 281: 978-980.
672 Furnes, H., Banerjee, N.R., Muehlenbachs, K., Staudigel, H. and de Wit, M., 2004. Early life
673 recorded in Archean pillow lavas. Science, 304: 578-581.
674 González, J.E., York, G.M. and Walker, G.C., 1996. *Rhizobium meliloti* exopolysaccharides:
675 Synthesis and symbiotic function. Gene, 179(1): 141-146.

676 Grantham, M.C. and Dove, P.M., 1996. Investigation of Bacterial-Mineral Interactions Using
677 Fluid Tapping Mode Atomic Force Microscopy. Geochimica et Cosmochimica Acta,
678 60(13): 2473 - 2480.
679 Hall, R.D. and Horn, L.L., 1993. Rates of hornblende etching in soils in glacial deposits of the
680 northern Rocky Mountains (Wyoming-Montana, USA); influence of climate and
681 characteristics of the parent material. Chemical Geology, 105: 17-29.
682 Hall, R.D. and Martin, R.F., 1986. The etching of hornblende grains in the matrix of alpine tills
683 and periglacial deposits. In: S.M. Colman and D.P. Dethier (Editors), Rates of chemical
684 weathering of rocks and minerals. Academic Press, Orlando, pp. 101-128.
685 Hamer, M., Graham, R.C., Amrhein, C. and Bozhilov, K.N., 2003. Dissolution of ripidolite (Mg,
686 Fe-Clorite) in organic and inorganic acid solutions. Soil Science Society of America
687 Journal, 67(2): 654-661.
688 Hamilton, J.P., Pantano, C.G. and Brantley, S.L., 2000. Dissolution of albite glass and crystal.
689 Geochimica et Cosmochimica Acta, 64(15): 2603-2615.
690 Hersman, L., Lloyd, T. and Sposito, G., 1995. Siderophore-promoted Dissolution of Hematite.
691 Geochimica et Cosmochimica Acta, 59(16): 3327 - 3330.
692 Hersman, L.E., 2000. The role of siderophores in iron oxide dissolution. In: D. Lovley (Editor),
693 Environmental Microbe-Metal Interactions. ASM Press, Washington, D. C., pp. 145 -
694 157.
695 Holmen, B.A. and Casey, W.H., 1996. Hydroxymate ligands, surface chemistry, and the
696 mechanism of ligand-promoted dissolution of goethite [a-FeOOH(s)]. Geochimica et
697 Cosmochimica Acta, 60: 4403-4416.

698 Honess, A.P., 1929. The theory of crystal etching and its significance in the classification of
699 crystals. Bulletin - PA State College Mineral Industries Experiment Station 3: 1-8.
700 Huang, P.M., 1989. Feldspars, olivines, pyroxenes, and amphiboles. In: J.B. Dixon and S.B.
701 Weed (Editors), Minerals in Soil Environments. Soil Sci. Soc. Am., Madison, pp. 975-
702 1050.
703 Kalinowski, B.E., Liermann, L.J., Brantley, S.L., Barnes, A. and Pantano, C.G., 2000. X-ray
704 photoelectron evidence for bacteria-enhanced dissolution of hornblende. Geochimica et
705 Cosmochimica Acta, 64(8): 1331-1343.
706 Kraemer, S.M. et al., 1999. Effect of hydroxamate siderophores on Fe release and Pb(II)
707 adsorption by goethite. Geochimica Cosmochimica Acta, 63: 3003-3008.
708 Larsen, B. and Haug, A., 1971. Biosynthesis of alginate. Part I. Composition and structure of
709 alginate produced by *Azotobacter vinelandii* (Lipman). Carbohydrate Research, 17(2):
710 287-296.
711 Lasaga, A.C. and Luttge, A., 2001. Variation of crystal dissolution rate based on a dissolution
712 stepwave model. Science, 291: 2400-2404.
713 Liermann, L.A., Barnes, A.S., Kalinowski, B.E., Zhou, X. and Brantley, S.L., 2000a.
714 Microenvironments of pH in biofilms grown on dissolving silicate surfaces. Chemical
715 Geology, 171: 1 - 6.
716 Liermann, L.J., Kalinowski, B.E., Brantley, S.L. and Ferry, J.G., 2000b. Role of bacterial
717 siderophores in dissolution of hornblende. Geochimica et Cosmochimica Acta, 64(4):
718 587-602.

719 Liermann, L.J., Marin, A., Guynn, R.L., Anbar, A. and Brantley, S.L., 2005. Production of a
720 molybdophore during metal-targeted dissolution of silicates by soil bacteria. Chemical
721 Geology: In Press.
722 Little, B.J., Wagner, P.A. and Lewandowski, Z., 1997. Spatial relationships between bacteria and
723 mineral surfaces, Geomicrobiology: Interactions Between Microbes and Minerals.
724 Reviews in mineralogy. Mineralogical Society of America, Washington, D.C., pp. 123-
725 159.
726 Lüttge, A., Bolton, E.W. and Lasaga, A.C., 1999. An interferometric study of the dissolution
727 kinetics of anorthite: The role of reactive surface area. American Journal of Science, 299:
728 652-678.
729 Lüttge, A. and Conrad, P.G., 2004. Direct observation of microbial inhibition of calcite
730 dissolution. APPLIED AND ENVIRONMENTAL MICROBIOLOGY, 70(3): 1627-
731 1632.
732 Madigan, M.T., Martinko, J.M. and Parker, J., 2000. Brock Biology of Microorganisms. Prentice
733 Hall, New Jersey, 991 pp.
734 Malinovskaya, I.M., Kosenko, L.V., Votselko, S.K. and Podgorskii, V.S., 1990. Role of Bacillus
735 mucilaginosus Polysaccharide in Degradation of Silicate Minerals. Mikrobiologiya,
736 59(1): 70 - 78.
737 Maurice, P., Forsythe, J., Hersman, L. and Sposito, G., 1996. Application of atomic-force
738 microscopy to studies of microbial interactions with hydrous Fe(III)-oxides. Chemical
739 Geology, 132: 33-43.

740 Maurice, P.A. et al., 2001. Direct observations of aluminosilicate weathering in the hyphoreic
741 zone of an Antarctic dry valley stream. Geochimica et Cosmochimica Acta, 66(8): 1335-
742 1347.
743 Medlin, J.H., Suhr, N.H. and Bodkin, J.B., 1969. Atomic absorption analysis of silicates
744 employing $LiBO_2$ fusion. Atomic Absorption Newsletter, 8(2): 25-29.
745 Mellott, N.P., Brantley, S.L. and Pantano, C.G., 2002. Topography of polished plates of albite
746 crystal and glass during dissolution. In: R. Hellmann and S.A. Wood (Editors), Water-
747 Rock Interactions, Ore Deposits, and Environmental Geochemistry: A Tribute to David
748 A. Crerar. The Geochemical Society, St. Louis, pp. 462.
749 Miller, W.P., Zelazny, L.W. and Martens, D.C., 1986. Dissolution of synthetic crystalline and
750 noncrystalline iron oxides by organic acids. Geoderma, 37(1): 1-13.
751 Morel, F.M.M. and Palenik, B., 1989. The aquatic chemistry of trace metals in biofilms. In:
752 W.G. Characklis and P.A. Wilderer (Editors), Structure and Function of Biofilms. J.
753 Wiley and Sons, New York, pp. 289-300.
754 Neilands, J.B., 1995. Siderophores: structure and function of microbial iron transport
755 compounds. Journal of Biological Chemistry, 270: 26723-26726.
756 Neilands, J.B. and Nakamura, K., 1991. Detection, determination, isolation, characterization and
757 regulation of microbial iron chelates. In: G. Winkelmann (Editor), CRC Handbook of
758 Microbial Iron Chelates. CRC Press, Boca Raton, Florida, pp. 1-14.
759 NIST, 1998. NIST Critically Selected Stability Constants of Metal Complexes Database. U.S.
760 Dept. of Commerce, Gaithersburg, MD, 42 pp.

761 Nordmark, E.L., Yang, Z., Huttunen, E. and Widmalm, G., 2005. Structrual studies of an
762 exopolysaccharide produced by *Streptococcus thermophilus* THS. Biomacromolecules, 6:
763 105-108.
764 Roane, T.M. and Kellogg, S.T., 1996. Characterization of bacterial communities in heavy metal
765 contaminated soils. Canadian Journal of Microbiology, 42: 593-603.
766 Rogers, J.R., Bennett, P.C. and Choi, W.J., 1998. Feldspars as a source of nutrients for
767 microorganisms. American Mineralogist, 83: 1532 - 1540.
768 Rohrer, J.S. and Olechno, J.D., 1992. Secondary isotope effect: The resolution of deuterated
769 glucoses by anion-exchange chromatorgaphy. Analytical Chemistry, 64: 914-916.
770 Rosenberg, D.A. and Maurice, P.A., 2003. Siderophore adsorption to and dissolution of kaolinite
771 at pH 3 to 7 and 22 C. Geochimica et Cosmochimica Acta, 67(2): 223-229.
772 Ruppe, C. and Duparee, A., 1996. Roughness analysis of optical films and substrates by atomic
773 force microscopy. Thin Solid Films, 288: 8-13.
774 Sawyer, L.K. and Hermanowicz, S.W., 1998. Detachment of biofilm bacteria due to variations in
775 nutrient supply. Water Science and Technology, 37(4-5): 211-214.
776 Schott, J., Berner, R.A. and Sjoberg, E.L., 1981. Mechanism of pyroxene and amphibole
777 weathering: I. Experimental studies of iron-free minerals. Geochimica et Cosmochimica
778 Acta, 45: 2123-2135.
779 Schwartzman, D.W. and Volk, T., 1991. Biotic enhancement of weathering and surface
780 temperatures on earth since the origin of life. Palaeogeogr. Palaeoclim. Palaeoecol., 90:
781 357-371.
782 Schwyn, B. and Neilands, J.B., 1987. Universal Chemical Assay for the Detection and
783 Determination of Siderophores. Analytical Biochemistry, 160: 47 - 56.

784 Sloneker, J.H. and Jeanes, A., 1962. Exocellular bacterial polysaccharide from Xanthomonas
785 campestris NRRL B-1459. Canadian Journal of Chemistry, 40: 2066-2071.
786 Staudigel, H., Chastain, R.A., Yayanos, A. and Bourcier, W., 1995. Biologically Mediated
787 Dissolution of Glass. Chemical Geology, 126: 147 - 154.
788 Suhr, N.H. and Ingamells, C.O., 1966. Solution technique for analysis of silicates. Analytical
789 Chemistry, 38: 730-734.
790 Sutherland, I., 1997. Microbial exopolysaccharides - structural subtleties and their consequences.
791 Pure and applied chemistry, 69(9): 1911-1917.
792 Sutherland, I.W., 2001. Biofilm exopolysaccharides: a strong and sticky framework.
793 Microbiology, 147(1): 3-9.
794 Templeton, A.S., Trainor, T.P., Spormmann, A.M. and Brown Jr., G.E., 2003. Selenium
795 speciation and partitioning within *Burkholderia cepacia* biofilms formed on α-Al_2O_3
796 surfaces. Geochimica et Cosmochimica Acta, 67(19): 3547-3557.
797 Thorseth, I.H., Furnes, H. and Tumyr, O., 1995. Textural and chemical effects of bacterial
798 activity on basaltic glass: an experimental approach. Chem. Geol., 119: 139-160.
799 Velbel, M.A., 1989. Weathering of Hornblende to Ferruginous Products by a Dissolution-
800 Reprecipitation Mechanism: Petrography and Stoichiometry. Clays and Clay Minerals,
801 37(6): 515 - 524.
802 Vig, J.R., 1992. Ultraviolet-Ozone Cleaning of Semiconductor Surfaces. Research and
803 Development Technical Report SLCET-TR-91-33, Army Research Laboratory.
804 Wang, H.-M., D., L. and Linhardt, R.J., 1991. Determination of the pK_a of glucuronic acid and
805 the carboxy groups of heparin by ^{13}C-nuclear-magnetic-resonance spectroscopy.
806 Biochemical Journal, 278: 689-695.

807 Watnick, P. and Kolter, R., 2000. Biofilm, city of microbes. Journal of Bacteriology, 182(10):
808 2675-2679.
809 Welch, S.A. and Vandevivere, P., 1994. Effect of Microbial and Other Naturally Occurring
810 Polymers on Mineral Dissolution. Geomicrobiology Journal, 12: 227 - 238.
811 White, A.F. and Brantley, S.L., 1995. Chemical weathering rates of silicate minerals: An
812 overview. In: A.F. White and S.L. Brantley (Editors), Chemical Weathering Rates of
813 Silicate Minerals. Reviews in mineralogy. Mineralogical Society of America,
814 Washington, D.C., pp. 1-22.
815 Wilderer, P.A. and Characklis, W.G., 1989. Structure and function of biofilms. In: W.G.
816 Characklis and P.A. Wilderer (Editors), Structure and Function of Biofilms. Wiley and
817 Sons, New York, pp. 5-17.
818 Winkelmann, G., 1991. Specificity of iron transport in bacteria and fungi. In: G. Winkelmann
819 (Editor), CRC Handbook of microbial iron chelates. CRC Press, Boca Raton, Florida, pp.
820 366.
821 Zazzera, L. and Evans, J.F., 1993. In situ internal reflection infrared study of aqueous
822 hydrofluoric acid and ultraviolet/ozone treated silicon (100) surfaces. Journal of Vacuum
823 Science & Technology, A11: 4934-4939.
824

825 **Figure Captions**

826 **Figure 1.** Release of Fe, Al, or Si (μM) from Fe-silicate glass surfaces to MM9 medium. **(a)** The
827 [Fe] in the bacteria-containing experiments is below the lower detection limits of the ICP-AES,
828 consistent with uptake of Fe by the bacteria. Fe release was comparable in all solutions without
829 DFAM, whereas the DFAM-containing solutions enhanced Fe release. Alginate + DFAM

solutions showed the greatest release. Similar trends are seen for **(b)** Al release and **(c)** Si release, except these elements were not completely removed from solution by the bacteria.

Figure 2. Fe/Si ratios of the upper ~100 Å of the hornblende glass surfaces measured by XPS. Error in the XPS measurements is estimated to be about 5% for Si and 10% for Fe. Measurements on replicate samples are shown as averages except for the blanks and controls, for which all replicates are shown. Sample variability is greater than the XPS measurement error for blanks: the highest and lowest Fe/Si ratios are bracketed by lines for the two blanks. This variability is used as the error on the samples. Standard deviations of the averaged values are within this variability range. The x-axis is arbitrary. Sample codes: A = alginate, X = xanthan gum, D = DFAM, B = inside dialysis bag, control = growth media only.

Figure 3. AFM height images of 10 x 10 μm areas of hornblende glass planchets. The vertical scale is ± 200 nm from the average plane (gray). Lighter and darker areas represent positive and negative topography, respectively, relative to the average plane of the surface. **(a)** Starting surfaces, or "blanks," were polished but not incubated in solution. AFM images of blanks reveal polishing scratches visible on all sample surfaces. **(b)** Control surfaces were polished and incubated in MM9 growth medium for 46 days and appear unchanged relative to blanks. **(c)** Surfaces exposed 240 μM DFAM in MM9 medium for 46 days reveal numerous, widely distributed etch pits (< 450 nm wide, < 60 nm deep). Pits were seen on un-scratched areas of the surfaces as well as along polishing scratches.

852 **Figure 4.** AFM height images of 10 x 10 μm areas of hornblende glass planchets. The vertical
853 scale is ± 200 nm from the average plane. Lighter and darker areas represent positive and
854 negative topography, respectively, relative to the average plane of the surface. **(a)** On surfaces
855 incubated in MM9 medium with xanthan gum or **(b)** alginate, polishing scratches appear slightly
856 more prominent than on control and blank surfaces (Fig. 3a-b). **(c)** When the siderophore DFAM
857 was combined with xanthan gum or **(d)** with alginate, etch pits, enlarged polishing scratches and
858 more prominently etched background texture was observed in AFM images.
859
860 **Figure 5.** Cross sections of AFM imaged surfaces exposed to **(a)** xanthan gum or **(b)** xanthan
861 gum and the siderophore DFAM. The white lines on the AFM images at the right of the figure
862 indicate the locations of the cross sections. The vertical scale is ± 50 nm.
863
864 **Figure 6. (a)** and **(b)** AFM height images of 10 x 10 μm areas of hornblende glass surfaces after
865 incubation with *Bacillus* sp. Vertical scale is ± 200 nm from the average plane, which is
866 represented by gray. Lighter and darker areas represent positive and negative topography,
867 respectively, relative to the average plane of the surface. The etch pits caused by the bacteria
868 tend to form in groups as shown here, leaving most of the surface un-pitted. Such "biopits" also
869 tend to be larger than those formed in abiotic experiments (Figs. 3-4).
870
871 **Figure 7.** Box and whisker statistical plot of root-mean-squared (RMS) roughness measured by
872 AFM on polished Fe-silicate sample surfaces. Sample codes: A = alginate, X = xanthan gum, D
873 = DFAM, B = inside dialysis bag, Bac = bacteria, Con = control (growth media only). Dotted
874 lines indicate the RMS roughness range of the untreated starting surfaces (blanks) measured on

875 15 surfaces. Boxes represent 25-75% of the data, whiskers (vertical lines) indicate 5-95% of the
876 data, X symbols bracket the range between 1 and 99% of the data and fall coincident with the
877 dash (–) symbols, which indicate the maximum and minimum values. Solid squares (■)
878 represent the mean.
879
880 **Figure 8.** VSI height image of a 164 x 124 μm area of a hornblende glass planchet incubated in
881 240 μM DFAM in MM9 growth medium. Vertical scale is ± 50 nm from the average plane. As
882 with the AFM height images, the lighter and darker areas represent positive and negative
883 topography, respectively, relative to the average plane of the surface, which is gray. The white
884 square in the bottom left corner of the image indicates the average size of the AFM scans (10 x
885 10 μm).
886

Buss Figure 1

Click here to download high resolution image

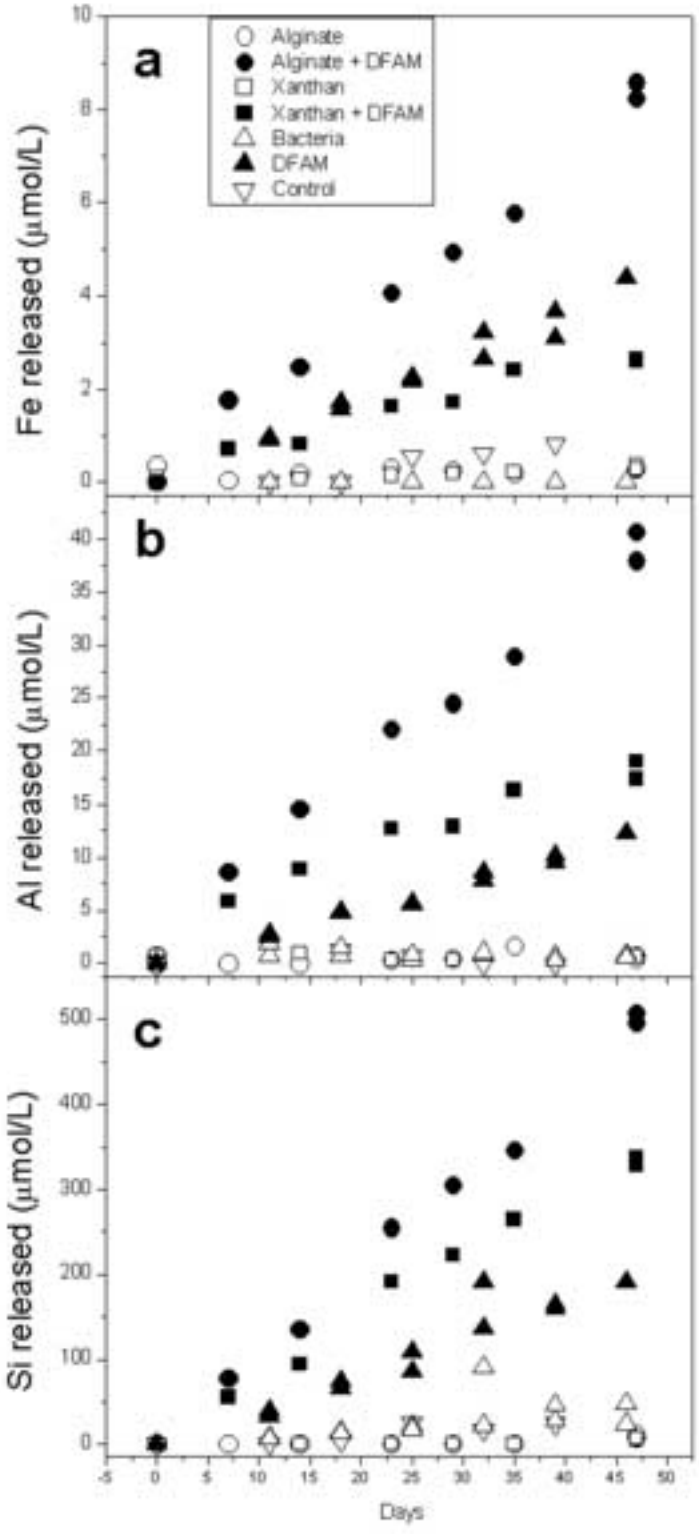

Figure 1

Buss Figure 2
Click here to download high resolution image

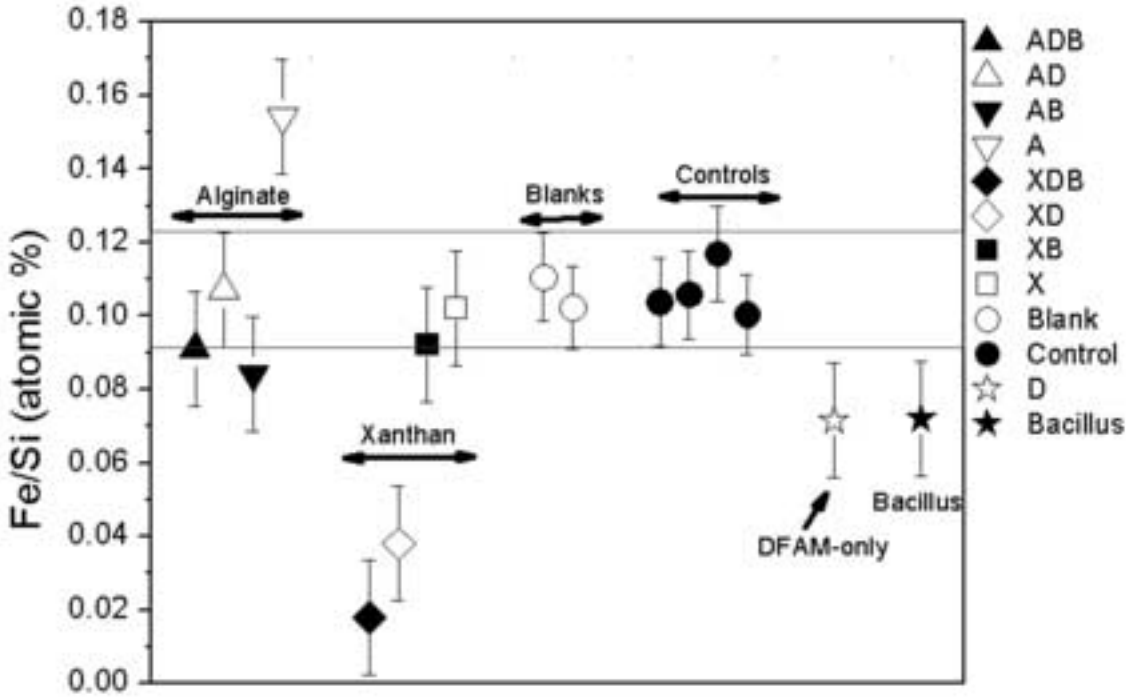

Figure 2

Buss Figure 3 (revised)
Click here to download high resolution image

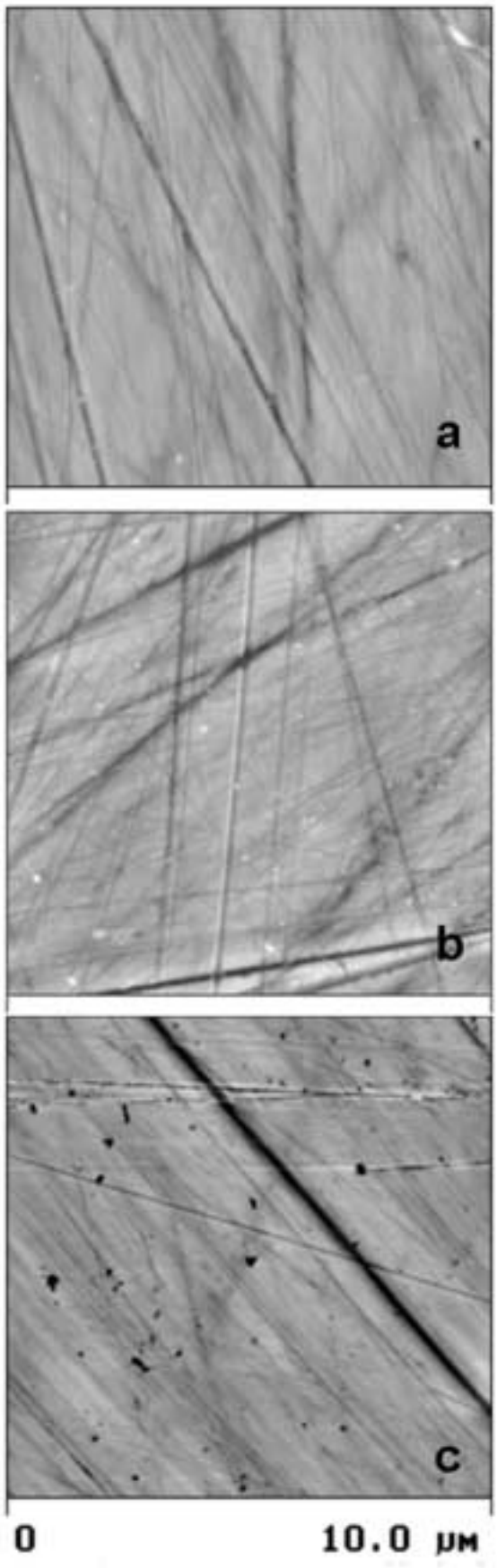

Figure 3

Buss Figure 4
Click here to download high resolution image

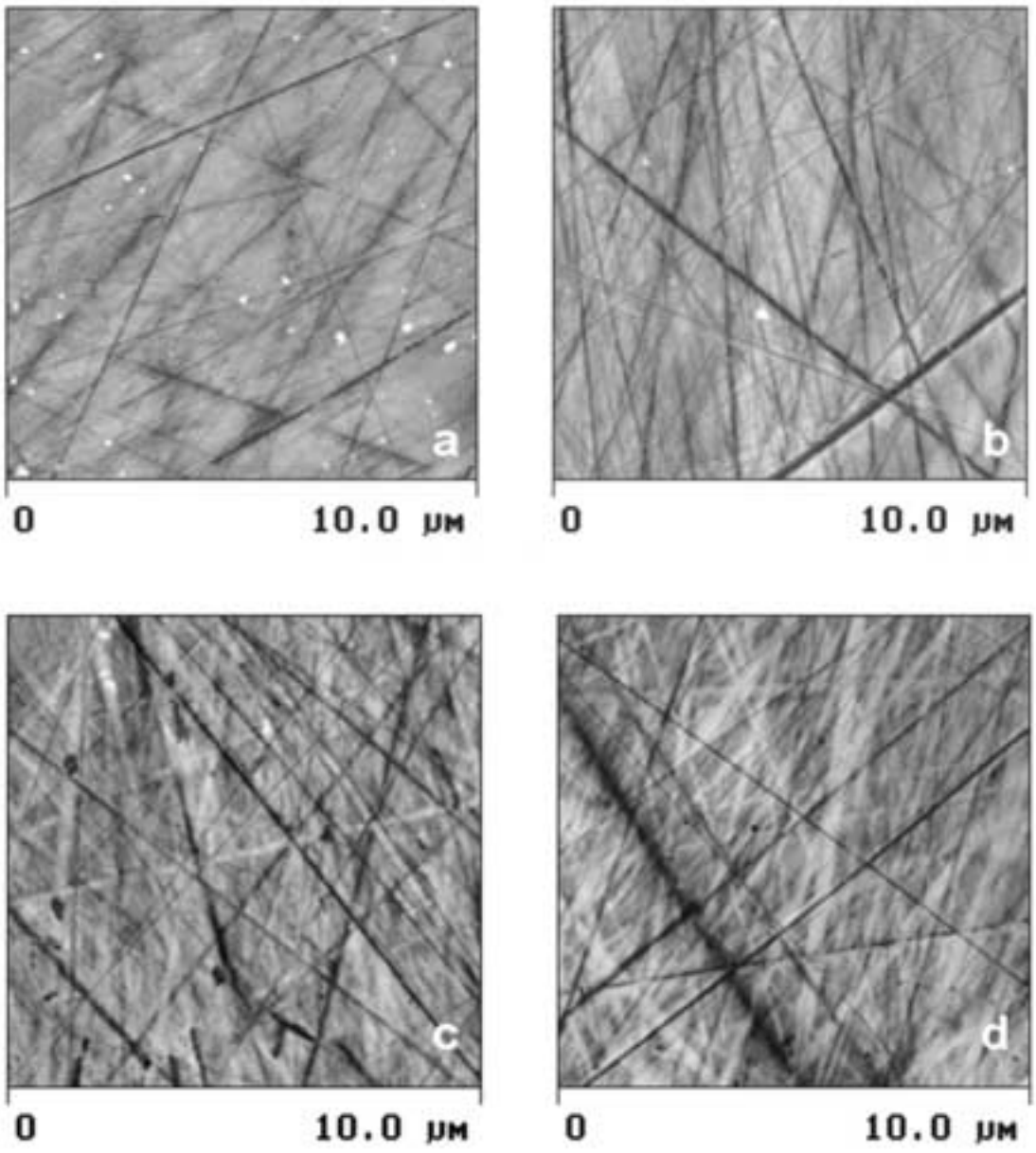

Figure 4

Buss Figure 5
Click here to download high resolution image

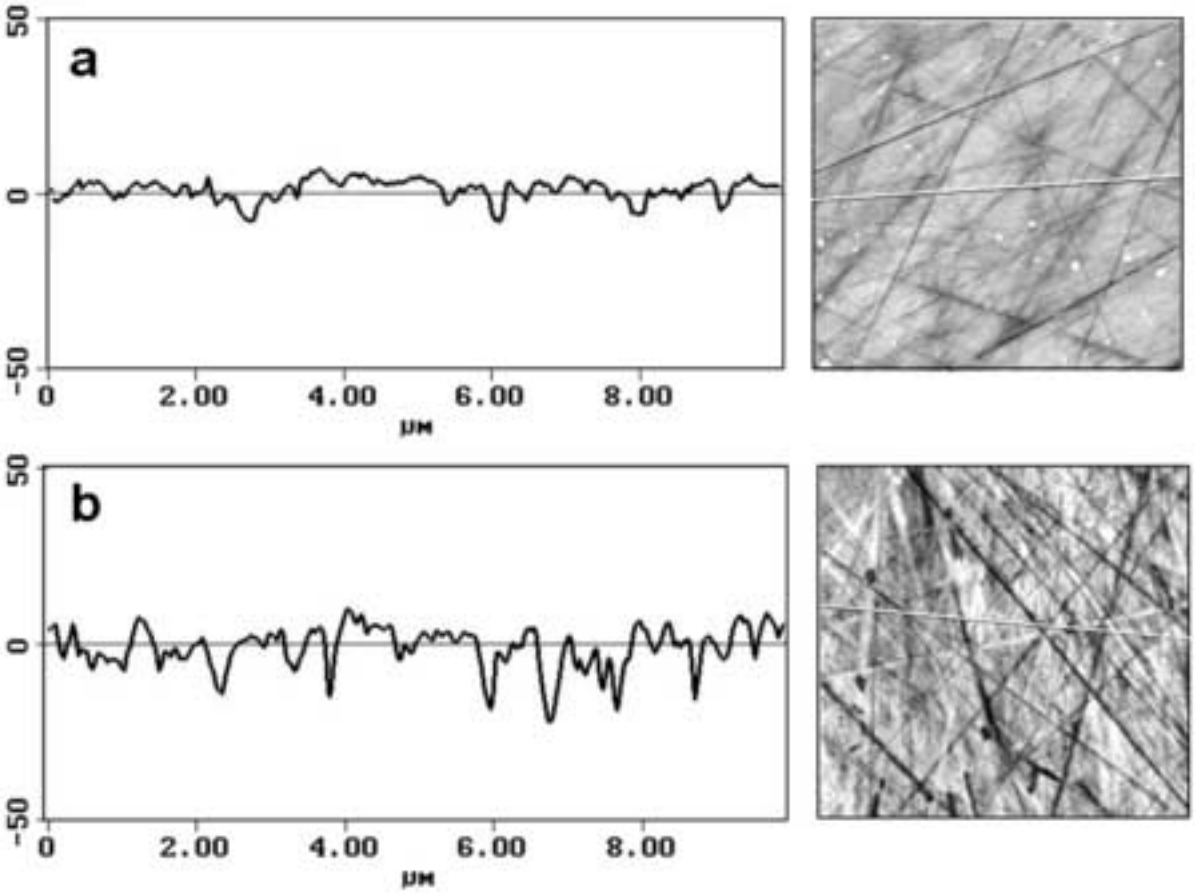

Figure 5

Buss Figure 6
Click here to download high resolution image

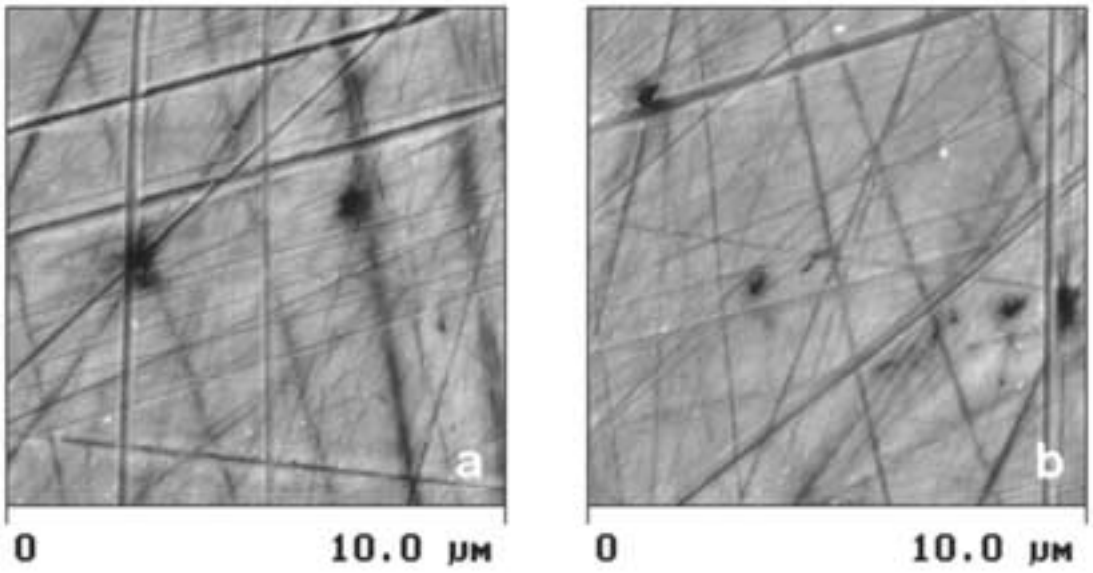

Figure 6

Buss Figure 7
Click here to download high resolution image

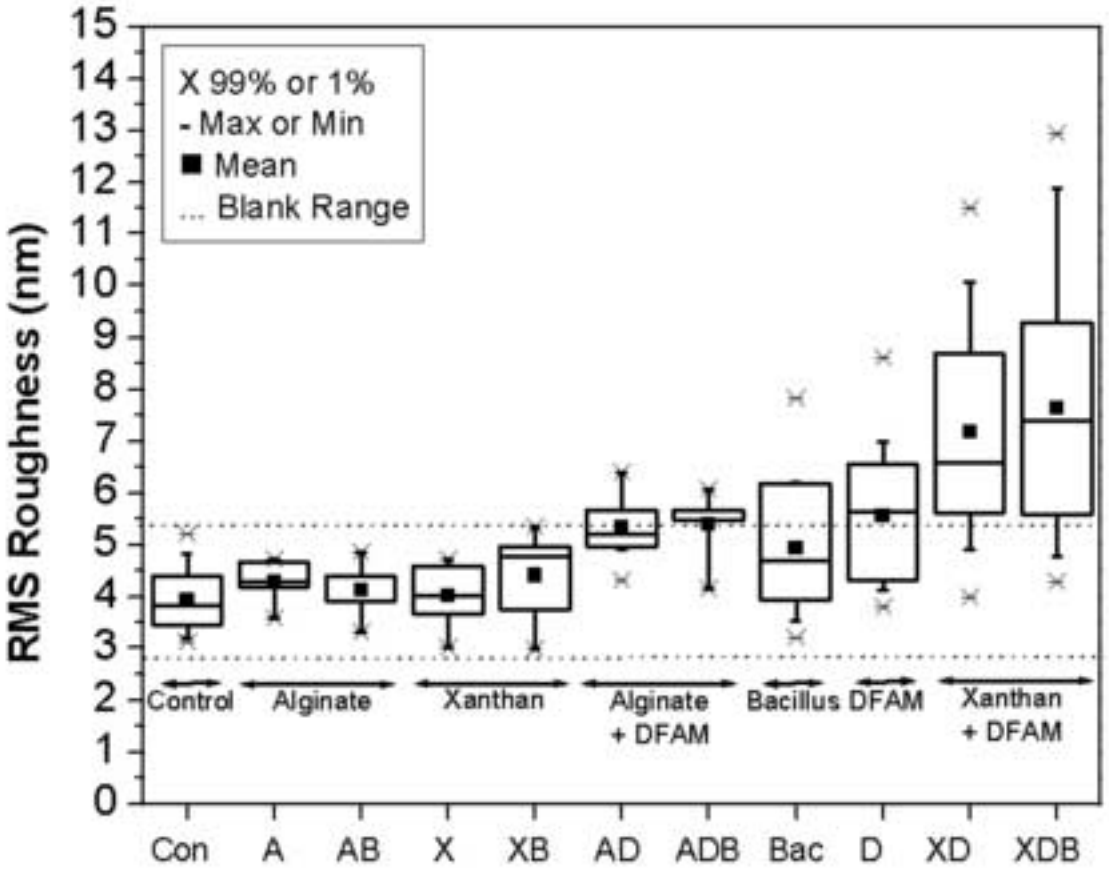

Figure 7

Figure 8 (revised)
Click here to download high resolution image

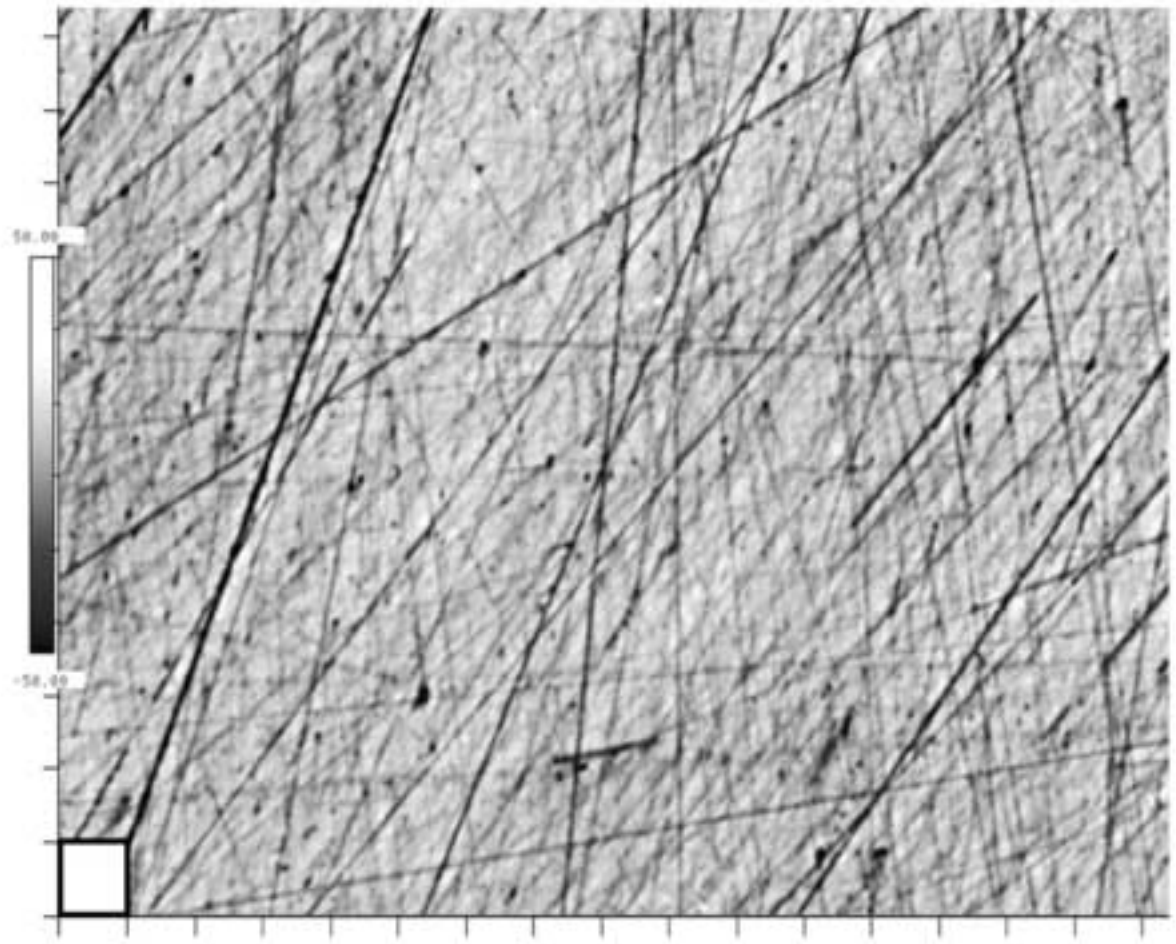

Figure 8

Table 1: Si, Fe, and Al released from hornblende glass

Experiment[a]	Days Incubation	[Si] µM	[Fe] µM	[Al] µM
Controls	39	24.6 ± 1.7	0.82 ± 0.00	bd
DFAM	39	159.2 ± 2.7	3.1 ± 0.3	9.5 ± 0.9
DFAM	46	191.5 ± 2.9	4.4 ± 0.4	12.3 ± 0.9
Bacteria	46	24.0 ± 1.4	bd	0.58 ± 0.33
Bacteria	46	47.5 ± 1.4	bd	0.84 ± 0.36
Alginate	47	7.4 ± 14.1	0.28 ± 0.08	0.67 ± 0.39
Alginate	47	12.0 ± 20.0	0.30 ± 0.06	0.50 ± 0.32
Xanthan Gum	47	6.2 ± 9.9	0.36 ± 0.06	0.55 ± 0.29
Xanthan Gum	47	7.5 ± 10.5	0.27 ± 0.04	0.62 ± 0.30
Alginate + DFAM	47	507.9 ± 39.7	8.6 ± 0.3	40.6 ± 0.39
Alginate + DFAM	47	496.3 ± 26.1	8.3 ± 0.5	37.9 ± 0.32
Xanthan + DFAM	47	328.3 ± 16.6	2.6 ± 0.1	17.4 ± 1.4
Xanthan + DFAM	47	337.7 ± 23.4	2.7 ± 0.1	19.0 ± 0.3

[a]Control experiments contained hornblende glass planchets incubated in Fe-free MM9 medium only. DFAM experiments contained hornblende glass planchets incubated in Fe-free MM9 medium with 240 µM desferrioxamine-B mesylate. Bacteria experiments contained hornblende glass planchets incubated in Fe-free MM9 medium with *Bacillus* sp. Alginate and xanthan gum experiments contained hornblende glass planchets incubated in MM9 medium with 0.1 g l^{-1} alginate or xanthan gum.

Table 2: Surface data

Experiment[a]	Days Incubation	Fe/Si (atomic %)[b]	Fe/Si (atomic %) *In dialysis bag*[c]	AFM[d] RMS (nm)	AFM RMS (nm) *In dialysis bag*	VSI[e] RMS (nm)
Blanks	0	0.102 – 0.110	na[f]	2.83 – 5.40	na	nd[f]
Controls	39	0.104 – 0.117	na	3.12 – 5.20	na	5.35 – 26.2
DFAM	39	0.072 ± 0.016	na	3.80 – 8.60	na	4.14 – 29.8
Bacillus	46	0.072 ± 0.016	na	3.22 – 7.33	na	5.19 – 21.5
Alginate	47	0.154 ± 0.016	0.084 ± 0.016	3.57 – 4.71	3.32 – 4.85	nd
Xanthan Gum	47	0.102 ± 0.016	0.092 ± 0.016	3.00 – 4.72	2.98 – 5.34	nd
Alginate + DFAM	47	0.107 ± 0.016	0.091 ± 0.016	4.32 – 6.39	4.16 – 6.06	nd
Xanthan + DFAM	47	0.038 ± 0.016	0.018 ± 0.016	3.98 – 11.5	4.28 – 12.9	nd

[a]Blanks are the starting material: polished hornblende glass planchets that were not incubated. Control experiments contained hornblende glass planchets incubated in Fe-free MM9 medium only. DFAM experiments contained hornblende glass planchets incubated in Fe-free MM9 medium with 240 µM desferrioxamine-B mesylate. Bacteria experiments contained hornblende glass planchets incubated in Fe-free MM9 medium with *Bacillus* sp. Alginate and xanthan gum experiments contained hornblende glass planchets incubated in MM9 medium with 0.1 g l^{-1} alginate or xanthan gum.

[b]Surface Fe relative to Si measured by XPS. Each XPS measurement is an average of three measurements on a single sample. Ranges are for given for replicate blanks and controls. Error in these values is based on measurement error of 5% for Si and 10% for Fe. This error is shown in Figure 2. Measurements on other replicate samples are reported as averages with error given as the sample variability based on the range and precision of measurement on the blanks.

[c]"In dialysis bag" indicates that the surfaces were protected from EPS by dialysis tubing.

[d]Range of AFM root mean square roughness values measured on 10 x 10 µm AFM images using Digital Instruments Nanoscope IIIa Controller software.

[e]Range of VSI root mean square roughness values calculated from raw numerical VSI data collected from 124 x 163 µm areas.

[f]na = not applicable, nd = not determined